Structure–activity relationships and molecular modelling of new 5-arylidene-4-thiazolidinone derivatives as aldose reductase inhibitors and potential anti-inflammatory agents

ARTICLE *in* EUROPEAN JOURNAL OF MEDICINAL CHEMISTRY · MAY 2014

Impact Factor: 3.45 · DOI: 10.1016/j.ejmech.2014.05.003 · Source: PubMed

10 AUTHORS, INCLUDING:

Rosanna Maccari
Università degli Studi di Messina
51 PUBLICATIONS **1,228** CITATIONS
SEE PROFILE

Rosaria Ottanà
Università degli Studi di Messina
73 PUBLICATIONS **1,435** CITATIONS
SEE PROFILE

Agostino Marrazzo
University of Catania
63 PUBLICATIONS **477** CITATIONS
SEE PROFILE

Adriana C. E. Graziano
University of Catania
30 PUBLICATIONS **135** CITATIONS
SEE PROFILE

European Journal of Medicinal Chemistry 81 (2014) 1–14

Contents lists available at ScienceDirect

European Journal of Medicinal Chemistry

journal homepage: http://www.elsevier.com/locate/ejmech

Original article

Structure–activity relationships and molecular modelling of new 5-arylidene-4-thiazolidinone derivatives as aldose reductase inhibitors and potential anti-inflammatory agents

Rosanna Maccari [a,1], Rosa Maria Vitale [b,1], Rosaria Ottanà [a,*], Marco Rocchiccioli [c], Agostino Marrazzo [d], Venera Cardile [e], Adriana Carol Eleonora Graziano [e], Pietro Amodeo [b], Umberto Mura [c], Antonella Del Corso [c]

[a] Dipartimento di Scienze del Farmaco e dei Prodotti per la Salute, University of Messina, Polo Universitario dell'Annunziata, 98168 Messina, Italy
[b] Istituto di Chimica Biomolecolare (ICB) – CNR, Comprensorio Olivetti, Ed. 70, Via Campi Flegrei 34, 80078 Pozzuoli, Napoli, Italy
[c] Dipartimento di Biologia, Unità di Biochimica, University of Pisa, Via S. Zeno 51, 56126 Pisa, Italy
[d] Department of Drug Sciences, Medicinal Chemistry Section, University of Catania, Viale A. Doria 6, 95125 Catania, Italy
[e] Department of Bio-medical Sciences, Section of Physiology, University of Catania, V.le A. Doria 6, 95125 Catania, Italy

ARTICLE INFO

Article history:
Received 23 December 2013
Received in revised form
28 April 2014
Accepted 1 May 2014
Available online 4 May 2014

Keywords:
Aldose reductase
Enzyme inhibitors
Anti-inflammatory agents
Molecular modelling
5-Arylidene-4-thiazolidinone derivatives
5-(carbamoylmethoxy)benzylidene-2-oxo/thioxo-4-thiazolidinone derivatives

ABSTRACT

A series of 5-(carbamoylmethoxy)benzylidene-2-oxo/thioxo-4-thiazolidinone derivatives (**6**–**9**) were synthesized as inhibitors of aldose reductase (AR), enzyme which plays a crucial role in the development of diabetes complications as well as in the inflammatory processes associated both to diabetes mellitus and to other pathologies.

In vitro inhibitory activity indicated that compounds **6**–**9a**–**d** were generally good AR inhibitors. Acetic acid derivatives **8a**–**d** and **9a**–**d** were shown to be the best enzyme inhibitors among the tested compounds endowed with significant inhibitory ability levels reaching submicromolar IC_{50} values.

Moreover, some representative AR inhibitors (**7a**, **7c**, **9a**, **9c**, **9d**) were assayed in cultures of human keratinocytes in order to evaluate their capability to reduce NF-kB activation and iNOS expression. Compound **9c** proved to be the best derivative endowed with both interesting AR inhibitory effectiveness and ability to reduce NF-kB activation and iNOS expression.

Molecular docking and molecular dynamics simulations were undertaken to investigate the binding modes of selected compounds into the active site of AR in order to rationalize the inhibitory effectiveness of these derivatives.

1. Introduction

Aldose reductase (AR) is an aldo-keto reductase present in the cytoplasm of most human cells. During the last three decades, a great deal of attention has been focused on this enzyme, since it was established that AR plays a crucial role in the development of chronic diabetic complications, such as neuropathy, nephropathy, cataracts, retinopathy, accelerated atherosclerosis and increased cardiovascular risk. Therefore, this enzyme has been assumed as an attractive target to prevent or treat these invalidating pathologies which are a serious health threat for diabetic patients [1–3]

AR is the first and rate-limiting enzyme of the polyol pathway in which it catalyses the NADPH-dependent reduction of glucose to sorbitol. Subsequently, sorbitol dehydrogenase converts sorbitol into fructose with concomitant reduction of NAD^+. Under normal glycaemic conditions, glucose is predominantly converted to glucose-6-phosphate by hexokinase and then enters the glycolytic pathway, whereas it is metabolized through the polyol pathway only in small amount, because AR has a relatively low affinity for this substrate. The major physiological role of AR appears to be the

Abbreviations: AGEs, advanced glycation-end products; AR, aldose reductase; ARI, aldose reductase inhibitor; COX-2, cyclooxygenase-2; DHN, 1,4-dihydroxynonene; DM, diabetes mellitus; GS-HNE, glutathione-4-hydroxy-*trans*-2-nonenal; HNE, 4-hydroxy-*trans*-2-nonenale; IFN-γ, interferon-gamma; NF-kB, nuclear factor-kB; NOS, nitric oxide synthase; PKC, protein kinase C; ROS, radical oxygen species; TNF-α, tumour necrosis factor-alfa.

* Corresponding author.
E-mail address: rottana@unime.it (R. Ottanà).

[1] These Authors contributed equally to this work.

http://dx.doi.org/10.1016/j.ejmech.2014.05.003
0223-5234/

removal of potentially toxic aldehydes generated during lipid peroxidation, such as 4-hydroxy-*trans*-2-nonenal (HNE), and their glutathione adducts (GS-HNE), which are reduced more efficiently than glucose by AR [4,5].

In contrast, under hyperglycaemic conditions, such as in diabetes mellitus (DM), up to one third of the total metabolized amount of glucose is shunted to the polyol pathway, in tissues possessing insulin-independent uptake of glucose, such as kidney, lens, retina, peripheral nerves [1]. The increased flux of glucose through the polyol pathway triggers multiple pathogenic mechanisms which underlie the development of degenerative diabetic complications. In fact, the intracellular accumulation of sorbitol, which is unable to cross cellular membranes, leads to osmotic imbalance, cell swelling and membrane permeability changes, mainly in the lens. Moreover, NADPH and NAD^+ deprivation is responsible for alterations in cellular redox potentials and, concomitantly, impairs the activity of enzymes such as nitric oxide synthase (NOS) and glutathione reductase. On the whole, these alterations result in cellular oxidative stress, as a consequence of the imbalance between increased production of radical oxygen species (ROS) and reduced intracellular antioxidant defense [1,4].

In addition, the increase in the levels of glycating agents such as fructose (end-product of the polyol pathway), dihydroxyacetone phosphate, glyceraldehyde-3-phosphate and methylglyoxal (deriving from increased glycolitic flux and fatty acid oxidation), enhances the intracellular formation of advanced glycation-end products (AGEs) [1]. AGEs in turn can cause pathological alterations in the functions of intracellular proteins and lead to further generation of ROS. Moreover, dihydroxyacetone phosphate can be converted to diacylglycerol which also contributes to increased oxidative stress through the abnormal activation of protein kinase C (PKC) [1].

All these AR-mediated biochemical alterations originate vascular damage and decreased nerve conduction velocity that result in microvascular and macrovascular pathologies as well as neuropathy. On this basis, the inhibition of AR may be an optimal strategy to counteract the development of chronic pathologies associated to DM, by blocking the activity of this central enzyme that mediates hyperglycemia-induced oxidative stress and consequent tissue and vascular alterations. Indeed, studies in animal models and in humans showed that AR inhibitors (ARIs) can prevent or slow down the progression of certain DM-associated disorders [6–8].

Unfortunately, despite the wide number of ARIs reported over the last three decades, clinical trials often provided disappointing results due mainly to pharmacokinetic drawbacks, adverse side effects or low in vivo efficacy. Currently, epalrestat (Fig. 1) is the only ARI available for therapy, whereas several other inhibitors, such as fidarestat (Fig. 1), have entered clinical trials [2,3,9,10].

Recently, advances in the understanding of the pathophysiological actions of AR have resulted in a renewed interest in the search for more efficacious and safer ARIs. In particular, it was established that AR is critically involved in inflammatory processes under both normoglycemic and diabetic conditions. This enzyme, which is overexpressed under various oxidative conditions, intervenes in multiple signalling pathways leading to inflammation and tissue degeneration. In fact, ROS determine lipid peroxidation and production of hydrophobic lipid-derived aldehydes, such as HNE and its glutathione adduct GS-HNE, which are reduced by AR by originating 1,4-dihydroxynonene (DHN) and GS-DHN [4,5]. This latter has been identified as a pivotal mediator of oxidative stress-induced activation of nuclear transcription factor-kappa B (NF-kB), which in turn regulates the transcription of numerous genes involved in inflammation, apoptosis, cell proliferation and angiogenesis, resulting in the synthesis of cytokines, growth factors, tumour necrosis factor-alfa (TNF-α), matrix metalloproteases, cyclooxygenase-2 (COX-2) and inducible NOS (iNOS) [4,5,11–13]. The latter can be induced by other transcription factors in addition to NF-kB [14]. Both AR-derived PKC activation and production of AGEs also activate NF-κB [1].

Accordingly, it was ascertained that AR inhibition prevents multiple inflammatory pathways [15–17]. Chronic, often subclinical, inflammation is a key component of both DM and its complications and, in particular, is closely related to microvascular and macrovascular damage. Thus, these findings further highlight the crucial role that AR inhibition could play in the management of DM-associated chronic pathologies.

AR was also shown to be overexpressed in different types of human cancers, such as colon, lung, breast tumours, and to play a critical role in mediating ROS-induced carcinogenesis [18]. In addition, it was demonstrated that AR can mediate myocardial ischaemic injury both in diabetic and normoglycemic animals [19,20].

On the whole, these findings suggest that ARIs could offer new therapeutic strategies for the treatment of various pathologies, besides DM and its complications, such as rheumatoid arthritis, sepsis, asthma, uveitis, atherosclerosis [11,16].

At the same time, new approaches have been stimulated to test ARIs in vivo by designing new trails suitable to assess the efficacy of these agents in preventing or counteracting chronic inflammation and vascular damage [4,21].

All these findings prompted us to pursue our search for new ARIs, which in the last few years allowed us to identify 5-arylidene-4-thiazolidinone derivatives (including compounds **1**–**4**, Fig. 1) as potent in vitro ARIs, some of which also endowed with antioxidant properties [22–28]. In our previous studies, we ascertained that the presence of an acetic chain on N-3 of the thiazolidinone ring is related to the highest levels of AR inhibitory activity, whereas the substituents inserted on the 5-arylidene moiety can modulate the effectiveness of these ARIs by interacting with the so-called “specificity pocket” of the AR active site [29]. In particular, the insertion of a carboxymethoxy chain on the 5-benzylidene ring was generally shown to be beneficial for activity by critically intervening in the binding to AR [23].

In addition, we found that the replacement of the carbonyl group in position 2 of the 2,4-thiazolidinedione scaffold of these previously reported ARIs with the bioisoster thiocarbonyl group can improve inhibitory efficacy [27].

In continuing our search, herein we report the synthesis, structure–activity relationships and docking studies of 5-(carbamoylmethoxy)benzylidene-2-oxo/thioxo-4-thiazolidinone derivatives (**6**–**9**, Fig. 2). They were designed by assuming the carbamoylmethoxy group as a non ionisable isoster of the carboxymethoxy chain. This replacement may improve the cellular permeability and, at the same time, favour the binding to AR active site via hydrogen bonds, as suggested by our previous docking studies performed with analogous 2-(5-arylidene-2,4-dioxothiazolidin-3-yl)acetamides (**4**, Fig. 1) [24].

Compounds **6**–**9** were evaluated as in vitro inhibitors of AR isolated from bovine lens. This enzyme displays a sequence homology of more than 86% with human AR [30]. In order to assess their anti-inflammatory potential, they were also assayed in cultures of human keratinocytes by evaluating their capability to reduce NF-kB activation and iNOS expression.

Molecular docking simulations into the AR active site were carried out in order to gain new insight concerning the possible binding modes of this class of ARIs.

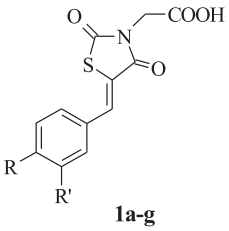

1a-g

	R	R'	IC_{50} (μM)
a	H	OCH_2COOH	0.23 (0.092-0.57)
b	OCH_2COOH	H	0.60 (0.40-0.90)
c	OCH_3	OCH_2COOH	0.20 (0.096-0.43)
d	OCH_2COOH	OCH_3	0.26 (0.10-0.70)
e	H	OCH_3	0.48 (0.092-0.57)
f	OH	OCH_3	0.56 (0.46-0.69)
g	OCH_3	OH	0.70 (0.68-0.72)

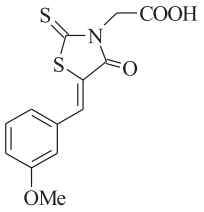

2 IC_{50} = 0.15 μM

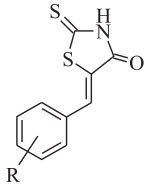

3a R = 3-OMe IC_{50} = 6.24 μM
3b R = 4-OMe IC_{50} = 5.23 μM

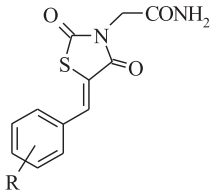

4

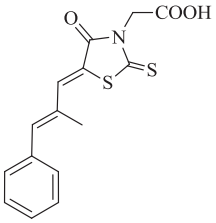

Epalrestat

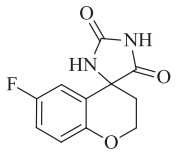

Sorbinil

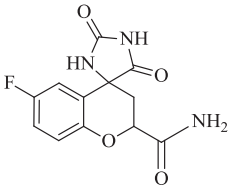

Fidarestat

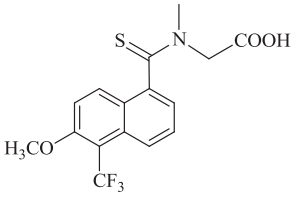

Tolrestat

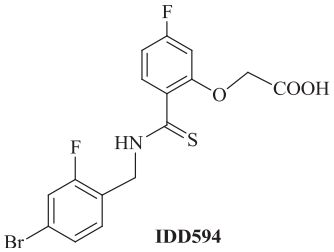

IDD594

Fig. 1. Structures of some 4-thiazolidinone derivatives **1** [23], **2**, **3** [27], **4** [24] active as AR inhibitors and of some known ARIs.

2. Results and discussion

2.1. Chemistry

Compounds **6a**–**d** were synthesized in good yield via Knoevenagel condensation starting from commercial 2,4-thiazolidinedione and arylaldehydes **5a**–**d** in refluxing ethanol in the presence of piperidine as base (Scheme 1). The reaction between commercial 2-thioxo-4-thiazolidinone and suitable aldehyde (**5a**–**d**) in glacial acetic acid and in the presence of sodium acetate at reflux provided pure 2-[(4-oxo-2-thioxothiazolidin-5-ylidenemethyl)phenoxy] acetamides (**7a**–**d**) in good yield (Scheme 2).

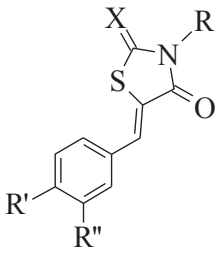

6-9 a-d

6 R = H, X = O
7 R = H, X = S
8 R = CH_2COOH, X = O
9 R = CH_2COOH, X = S

	R'	R''
a	H	OCH_2CONH
b	OCH_2CONH	H
c	OCH_3	OCH_2CONH
d	OCH_2CONH	OCH_3

Fig. 2. Structures of compounds **6**–**9**.

Although commercially available, 2-(formylaryloxy)acetamides (**5a**–**d**) were prepared by reaction of the appropriate hydroxybenzaldehyde and 2-chloroacetamide in refluxing acetonitrile in the presence of potassium carbonate (Scheme 1) (see Supplementary data).

The multi-step synthesis of (5-arylidene-2,4-dioxothiazolidin-3-yl)acetic acids **8a**–**d** is depicted in Scheme 1. A mixture of commercial 2,4-thiazolidinedione and methyl bromoacetate in the presence of potassium carbonate in boiling acetone afforded (2,4-dioxothiazolidin-3-yl)acetic acid methyl ester which was

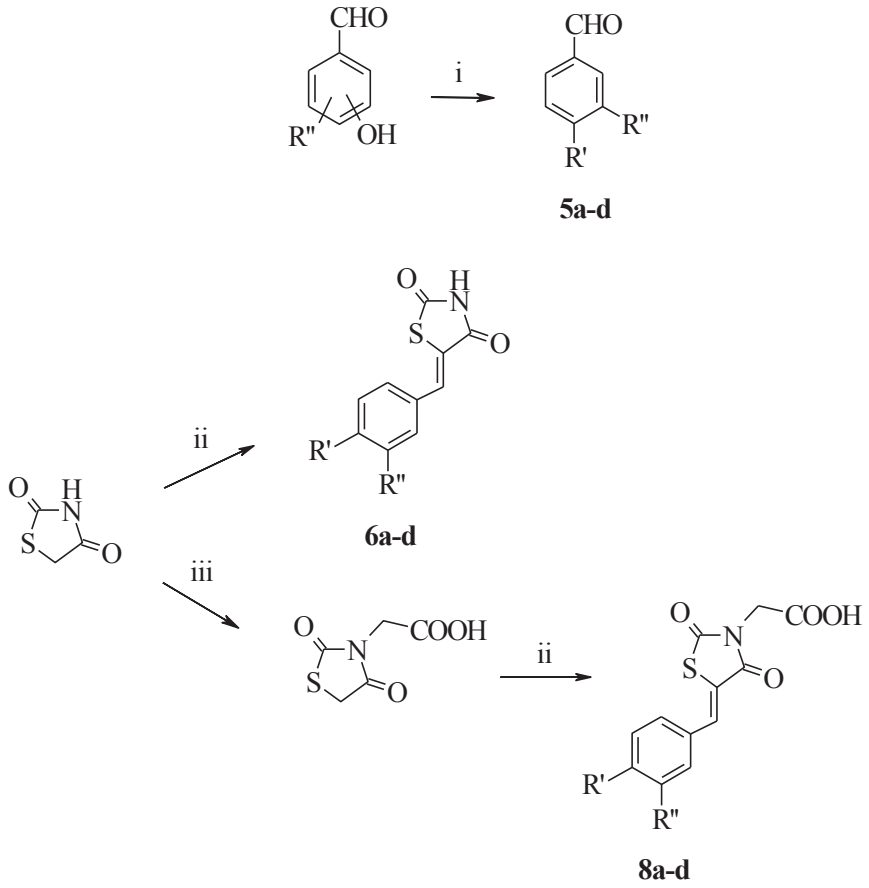

Scheme 1. Synthesis of compounds **6a**–**d** and **8a**–**d**. Reagents and conditions: i) $ClCH_2CONH_2$, K_2CO_3, CH_3CN, Δ; ii) Ar-CHO (**5a**–**d**), $C_5H_{11}N$, EtOH, Δ; iii) a) $BrCH_2COOCH_3$, K_2CO_3, acetone, Δ; b) CH_3COOH, HCl, Δ.

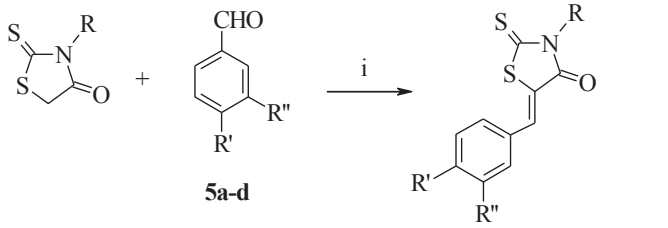

Scheme 2. Synthesis of compounds **7a**–**d** and **9a**–**d**. Reagents and conditions: i) CH_3COONa, CH_3COOH, Δ.

hydrolysed to corresponding acetic acid **10** by refluxing in a mixture of glacial acetic acid and HCl [22]. Finally a refluxing mixture of compound **10** and suitable aldehyde (**5a**–**d**) in the presence of piperidine in ethanol afforded compounds **8a**–**d** (Scheme 1).

(5-Arylidene-4-oxo-2-thioxothiazolidin-3-yl)acetic acids (**9a**–**d**) were obtained by the reaction of commercial (4-oxo-2-thioxothiazolidin-3-yl)acetic acid and appropriate aldehyde (**5a**–**d**) in refluxing glacial acetic acid and sodium acetate mixture (Scheme 2).

The structure of all synthesized compounds was unambiguously assigned on the basis of analytical and ^1H and ^{13}C NMR spectroscopy data. In the ^1H NMR spectra, the presence of one singlet at 7.55–7.88 ppm attributable to the CH methylidene proton proved to be significant in assigning the structure of compounds **6**–**9**. In addition the resonance of the methylene protons of the carbamoylmethoxy group resulted in a singlet ranging between 4.48 ppm and 4.73 ppm. In the ^1H NMR spectra of compounds **8** and **9** a diagnostic singlet appears attributable to the methylene protons on N-3 resonating at chemical shifts ranging between 4.34 and 4.55 ppm. In ^{13}C NMR spectra of compounds **6**–**9**, the methylene carbon of the carbamoylmethoxy group gave rise to a signal in the range from 66.6 to 67.6 ppm. Besides, in ^{13}C NMR spectra of acetic acids **8** and **9** the methylene carbon on N-3 resonated at 42.2–42.3 and 45.0–45.1, respectively.

On the basis of previously acquired X-ray diffraction analysis [28,31] as well as NMR spectroscopy data of analogous derivatives [22–28,31], the newly synthesized compounds **6**–**9** were obtained solely as *Z* diastereoisomers. In fact, NMR spectra showed in all cases only one set of signals and no isomerization at the C]C exocyclic double bond was subsequently observed.

2.2. Aldose reductase in vitro inhibition

The in vitro AR inhibitory activity of compounds **6**–**9 a**–**d** (Tables 1 and 2) was evaluated by using highly purified AR from bovine lenses [32]. Sorbinil and epalrestat (Fig. 1) were employed as reference drugs.

All tested compounds **6**–**9** were shown to be generally interesting AR inhibitors reaching up to submicromolar IC_{50} values. Entirely consistent with previous SARs outlined for this class of ARIs [22–28], (5-arylidene-2,4-dioxothiazolidin-3-yl)acetic acids (**8a**–**d**) and corresponding 2-thioxo isosters **9a**–**d** were showed to be the best ARIs among the tested compounds.

Moreover (5-arylidene-4-oxo-2-thioxothiazolidin-3-yl)acetic acids (**9a**–**d**) were even more active than both reference drugs by inhibiting the enzyme with IC_{50} values ranging from 0.11 μM to 0.13 μM (Table 2).

The acetic acid group on N-3 once again proved to play a critical role in the binding of compounds **8** and **9** to the AR catalytic site by resulting in the reduction of IC_{50} values up to one hundred times in comparison with N-unsubstituted compounds **6** and **7**. Among acetic acid inhibitors (compounds **8** and **9**) the differences of IC_{50} values were negligible, except for compound **8a** which showed to be twice less active than analogues **8b**–**d**. Compounds **6** and **7** produced level of enzyme inhibition in a wider range between 8.65 μM and 33.9 μM. These results highlight the pivotal role of the acetic group that thwarts the effects exerted by the substituents on 5-arylidene moiety.

Moreover the enzymatic inhibition results suggested that the 2-thioxo-4-thiazolidinone core (compounds **7a**–**d** and **9a**–**d**) may establish more favourable interactions with the enzyme in comparison to the isosteric 2,4-thiazolidinedione one (compounds **6a**–

Table 1
In vitro bovine lens AR inhibitory activity of compounds **6a**–**d** and **7a**–**d**.

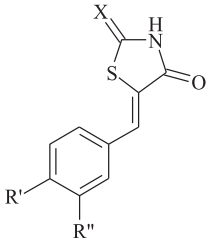

Compd	X	R′	R″	IC_{50} (μM)
6a	O	H	OCH_2CONH_2	21.5 (14–29)
6b	O	OCH_2CONH_2	H	40%[a]
6c	O	OCH_3	OCH_2CONH_2	22.6 (12.1–33.1)
6d	O	OCH_2CONH_2	OCH_3	33.9 (21.9–45.9)
7a	S	H	OCH_2CONH_2	8.65 (5.70–11.6)
7b	S	OCH_2CONH_2	H	34%[a]
7c	s	OCH_3	OCH_2CONH_2	9.20 (7.70–10.70)
7d	S	OCH_2CONH_2	OCH_3	11.6 (5.23–18.0)
Sorbinil				2.0 (1.70–3.50)
Epalrestat				0.17 (0.033–0.16)

[a] % inhibition at 50 μM.

Table 2
In vitro bovine lens AR inhibitory activity of compounds **8a**–**d** and **9a**–**d**.

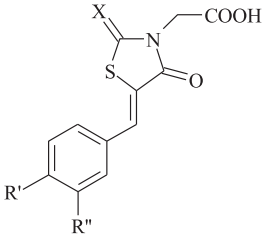

Compd	X	R′	R″	IC_{50} (μM)
8a	O	H	OCH_2CONH_2	1.01 (0.71–1.43)
8b	O	OCH_2CONH_2	H	0.56 (0.41–0.76)
8c	O	OCH_3	OCH_2CONH_2	0.52 (0.39–0.67)
8d	O	OCH_2CONH_2	OCH_3	0.50 (0.43–0.58)
9a	S	H	OCH_2CONH_2	0.13 (0.07–0.18)
9b	S	OCH_2CONH_2	H	0.13 (0.06–0.21)
9c	S	OCH_3	OCH_2CONH_2	0.13 (0.09–0.17)
9d	S	OCH_2CONH_2	OCH_3	0.11 (0.08–0.15)
Sorbinil				2.0 (1.70–3.50)
Epalrestat				0.17 (0.03–0.16)

d and **8a**–**d**), being equal the substituent in the 5-arylidene moiety (Tables 1 and 2).

The removal of the substituent on N-3 stresses the role played by the 5-arylidene moiety in the interaction with the enzyme. Comparing the inhibitory effectiveness of compounds **6** and **7** demonstrated that the carbamoylmethoxy group plays a critical role when inserted in the *meta* position. In fact compounds **6a**, **6c**, **7a** and **7c** showed to be better inhibitors than the corresponding *para* substituted analogues (**6b**, **6d**, **7b** and **7d**).

The introduction of the methoxy group also resulted to be favourable particularly in the *meta* position. Compounds **6d** and **7d**, 3-methoxy-4-carbamoylmethoxybenzylidene substituted (IC_{50} 33.9 μM and 11.6 μM, respectively), were more active in comparison with compounds **6b** and **7b**, 4-carbamoylmethoxybenzylidene substituted (40% and 34% inhibition at 50 μM, respectively), whereas the effect of the methoxy group in the *para* position (compounds **6c** and **7c**) was showed to be indifferent on enzymatic affinity (Table 1).

The replacement of 3/4-carboxymethoxy group (compounds **1a**–**d**, Fig. 1) [23] with the non ionisable carbamoylmethoxy one (compounds **8a**–**d**) on 5-arylidene moiety resulted generally in reduction of inhibitory activity (Table 2). Although compounds **8a**–**d** exerted interesting AR inhibition at submicromolar dose, they proved to be generally up to five times less active than carboxymethoxy isosters **1a**–**d**.

Starting from the previously reported [5-(3-methoxybenzylidene)-2,4-dioxothiazolidin-3-yl]acetic acid (**1e**, $IC_{50} = 0.48$ μM), the insertion of the carboxymethoxy group in *para* position was favourable for the AR inhibition providing compound **1d** endowed with $IC_{50} = 0.26$ μM (Fig. 1) [23], while the corresponding carbamoyl substituted analogue maintained the same level of activity (compound **8d** $IC_{50} = 0.50$ μM).

Comparing the activity of 4/3-hydroxybenzylidene analogues **1f** and **1g** (Fig. 1) with the corresponding carboxymethoxy (**1c** and **1d**) and carbamoylmethoxy (**8c** and **8d**) derivatives highlights that the introduction of the carboxymethoxy group on the 5-arylidene moiety (**1c**, **1d**) is advantageous for the interaction with the enzyme determining a reduction of the IC_{50} values of about two times [23], while its replacement with the carbamoylmethylene group is indifferent on inhibitory effectiveness (**8c**, **8d**).

In the series of 2-thioxo-4-thiazolidinone derivatives **7** and **9,** the introduction of the carbamoylmethoxy group in the *para* or *meta* position of previously reported compounds **2**, **3a**, **3b** (Fig. 1) [27] was either indifferent or unfavourable for the inhibitory effectiveness. In fact the inhibitory effectiveness of compounds **2** ($IC_{50} = 0.15$ μM) and **9d** ($IC_{50} = 0.11$ μM) was comparable while, among N-unsubstituted analogues (compounds **7**), the introduction of the carbamoylmethoxy group was detrimental for the enzyme affinity (cf. compounds **3a** and **7d**).

2.3. Molecular modelling

A combined approach of molecular docking and molecular dynamics (MD) simulations was undertaken to investigate the binding modes of compounds **6**, **7** and **9** into the active site of AR in order to rationalize the inhibitory effectiveness of these series of compounds which bear the same substituents on the 5-arylidene moiety but differ each other either for the presence of a carboxylic acid group on N-3 (**9** vs. **7**), or for the nature of the heterocyclic ring (**6** vs. **7**). Docking calculations were performed on the best inhibitors among 2-thioxo-4-thiazolidinones **7** and **9**, either containing the acid acetic group in position 3 (compound **9d**) or N-unsubstituted (compound **7a**), and among N-unsubstituted 2,4-thiazolidinediones **6** (compound **6a**). Compounds **7b** and **7d** were also evaluated since compound **7b**, despite containing the favourable 2-thioxo-4-thiazolidinone scaffold, exhibited the worst inhibitory properties among all studied compounds, but, upon introduction of a methoxy group in position 3 of the 5-arylidene ring, corresponding compound **7d** substantially recovered the activity of series **7**. In this view, the comparison between the docking properties of **7b** and **7d** also provided an assessment of the ability of the computational approach in discriminating between "good" and "bad" inhibitors.

AR binding site comprises two sub-pockets, the so-called "anionic binding site" encompassing the residues involved in catalysis (Tyr48, Lys77, and His110) along with the nicotinamide moiety of the cofactor $NADP^+$, and the "specificity pocket", formed by Trp111, Phe122, Trp219, Cys298, Ala299, Leu300, Ser302 and Cys303 [29]. Since the "specificity pocket" can adopt different conformations depending on the shape of the bound ligand, mainly due to the flexibility of the Cys298–Cys303 region, the three most diverging X-ray AR structures (from complexes with Fidarestat, Tolrestat and IDD594, respectively, Fig. 1) were used in molecular docking calculations. MD simulations of selected complexes (see details in the experimental section) were then performed both to assess the overall stability of the binding modes and to "merge" the different protein starting conformations, allowing protein rearrangements. The emerging features from a compared analysis of all the selected and refined complex structures allowed the classification of the binding modes in families and subfamilies, based on the occurrence of:

1) For all ligands, two main docking modes substantially independent on enzyme conformations and dependent on the inhibitor part that points toward the anionic binding site, either the thiazolidinone ring (hereinafter referred to as RING mode), or the amide group (AMD mode);
2) For compounds **7** and **9**, featuring a thiocarbonyl group in position 2 and a carbonyl group in position 4, two ring orientations, with the carbonylic oxygen atom pointing alternatively inward (RING-Oin) or outward (RING-Oout) respect to the enzyme binding pocket;
3) For those ligands such as **7a** and **6a** bearing the carbamoylmethoxy substituent in the meta position of the 5-arylidene ring, two different aryl group orientations (observed after MD, since docking provided somewhat intermediate orientations), referred to as AMD-m1 and AMD-m2, while in **7b**, where the amide group is present in para position, only a single orientation, referred to as AMD-p, was detected;
4) In all AMD poses, two possible amide group rotameric states, giving rise to two different H-bond patterns between the polar atoms of 3-carbamoylmethoxy group and protein Tyr48/His110/Trp111 side-chains, featuring contacts either of inhibitor ether oxygen with Trp111 and inhibitor carbonyl oxygen with Tyr48 (AMD-*x*-1, where x = m1, m2 or p), or of inhibitor carbamoyl oxygen with protein Tyr48 and ligand carbamoyl hydrogen with protein His110 (AMD-*x*-2).

Among N-unsubstituted inhibitors (**6a**, **7a**, and **7b**) subsequent MD simulations were performed on both RING and AMD modes. However, for compounds **7**, although both RING-Oin and RING-Oout orientations were simulated, only the former will be discussed, since it gave rise to H-bonds with the active site not observed in the latter. For compound **9d** only the RING mode was simulated, since the carboxylate moiety in position 3 of 2-thioxo4-thiazolidinone ring clearly can not form any ionic interaction with the active site when in the AMD orientation.

2.3.1. AR–7a complex

A MD trajectory analysis of AR–**7a** complexes shows that both RING and AMD orientations are stable over the entire simulated

period (20ns). In the RING pose the ligand formed stable H-bonds with His110 and Trp111, through N–H and the carbonyl group respectively. The exocyclic sulphur atom was involved in van der Waals interactions with Val47, Tyr48 and Trp20. The aryl group formed stable H-bond interactions through both amide and ether oxygens with backbone NH atoms of Ala299 and Leu300, respectively, thus anchoring the arylidene group to the Cys298–Leu301 loop of the specificity pocket. In this orientation, the benzylidene ring lay between Trp219 and Leu300 side-chains. During MD simulation a water molecule got trapped and became resident in the anionic binding site, by forming a stable H-bond with Tyr48 (Fig. 3A). The presence of a resident water molecule was still observed after a MD resubmission with a different random seed, thus suggesting that it may represent a characteristic feature of this system. The interaction energy between the resident water molecule and the protein–ligand complex, calculated on average on the last 10 ns of trajectory, was −13.9 ± 1.9 kcal mol^{-1}, thus contributing appreciably to the overall complex stabilization (Table 3).

Table 3
Mean total AR–ligand interaction energies (kcal mol^{-1}) calculated over last 10 ns of MD simulations for different orientations of **9d**, **7a**, **7b**, **7d** and **6a** in their complexes with AR.[a]

Ligand	Orientation	Mean protein–ligand interaction energy (kcal mol^{-1})
6a	RING	−51.95 (±6.24)
	AMD-m1	−41.08 (±4.27)
	AMD-m2	−52.04 (±3.25)
7a	RING	−50.92 (±3.97)
		−13.94 (± 1.87) water
	AMD-m1	−42.77 (±3.28)
	AMD-m2	−54.27 (±3.05)
7b	AMD-p-1	−41.20 (±3.80)
	AMD-p-2	−40.03 (±3.36)
7d	RING	−46.55 (±7.39)
	AMD-p	−46.20 (±4.84)
9d	RING-Oin	−120.98 (±9.17)
	RING-Oout	−117.36 (±9.60)

[a] In parentheses the corresponding rmsd values are shown. For the RING orientation of AR–**7a** the total interaction energy of a resident water molecule with AR and ligand (*italicized*) is also reported. Herein, AR also includes NADP$^+$.

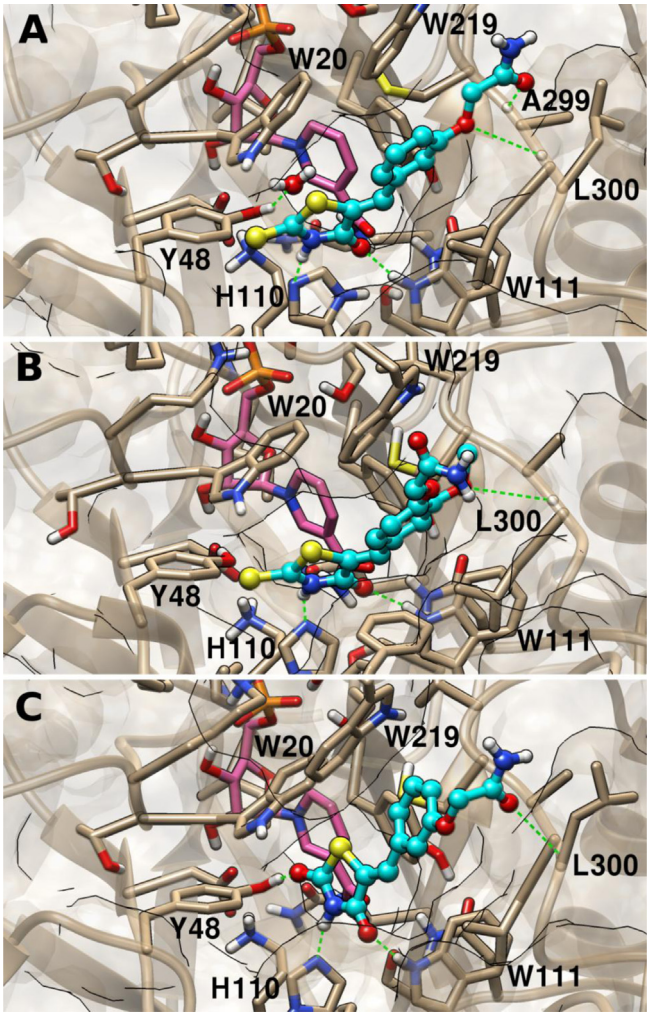

Fig. 3. Views of the binding site in modelled AR–ligand complexes after 20 ns of MD. The RING modes for **7a** (A), **7d** (B) and **6a** (C) are shown using a beige ribbon plus selected (within 5 Å from ligand) stick sidechain representation for AR, pink sticks for NADP$^+$ and cyan ball-and-stick for ligands. For all molecules only polar hydrogens are shown. Heteroatoms and polar hydrogens are coloured according to a standard scheme (red for oxygen, blue for nitrogen, yellow for sulphur and white for hydrogen). Intermolecular H-bonds are shown as green dotted-lines. (For interpretation of the references to colour in this figure legend, the reader is referred to the web version of this article.)

In the AMD orientation, the two different arrangements of the m-substituted aryl group exhibited considerable energetic differences, AMD-m1 being less stable than AMD-m2 (Table 3). In fact, while in AMD-m1 compound **7a** only formed hydrophobic contacts with Leu300 and Cys298 side-chains and a π-stacking between the 2-thioxo-4-thiazolidinone ring and Phe122 side-chain, in AMD-m2, in addition to a π-stacking of the heterocycle with Trp219 and to hydrophobic contacts of the 5-arylidene group with Trp20 and Leu300 side-chains, the esocyclic oxygen atom in position 4 engaged stable H-bonds with the backbone NH of Ala299 and Leu300 (Fig. 4A). On the contrary, protein–ligand interaction energies did not exhibit appreciable differences between AMD-*x*-1 and AMD-*x*-2, since the interactions of the amide group with the protein were almost isoenergetic between the two modes and the amide orientation itself did not affect other interactions of inhibitors (data not shown). During MD simulations AMD-*x*-1/AMD-*x*-2 interconversion was also observed.

2.3.2. AR–7b complex

Differently from what observed for AR–**7a** complex, the RING orientation of compound **7b** was not stable during MD simulation, where a lost of stabilizing H-bonds in the anionic binding site was observed (Fig. 5). The simulation was repeated using another ligand RING pose and also in this case the complex dissociated during MD (data not shown). Conversely, both AMD poses remained stable over the same simulated period (with their aryl group adopting the AMD-p orientation) resembling **7a** AMD-m2 rather than AMD-m1 one because of the observed π-stacking of the heterocycle with Trp219 (Fig. 4B). However, this pose was less stable than the corresponding AMD-m2 observed for **7a** since the different position of the functional group in the aryl moiety did not allow the occurrence of stabilizing H-bonds with the protein (Table 3).

2.3.3. AR–7d complex

Compound **7d** was stable in both RING and AMD orientations. In the RING pose, the aryl group formed alternatively π-stacking with Phe122 or with Trp219, where the methoxy group engaged H-bond interactions with backbone NH atoms of Ala299 or Leu300, similarly to the carbamoyl group of **7a** (Fig. 3B). In AMD orientation, the aryl group of **7d** adopted the AMD-p orientation already described for **7b**, but with additional hydrophobic contacts formed by the methoxy group with Trp20, Val47 and Phe122 that provided an additional complex stabilization of almost 5 kcal mol^{-1} over **7b** (Fig. 4C).

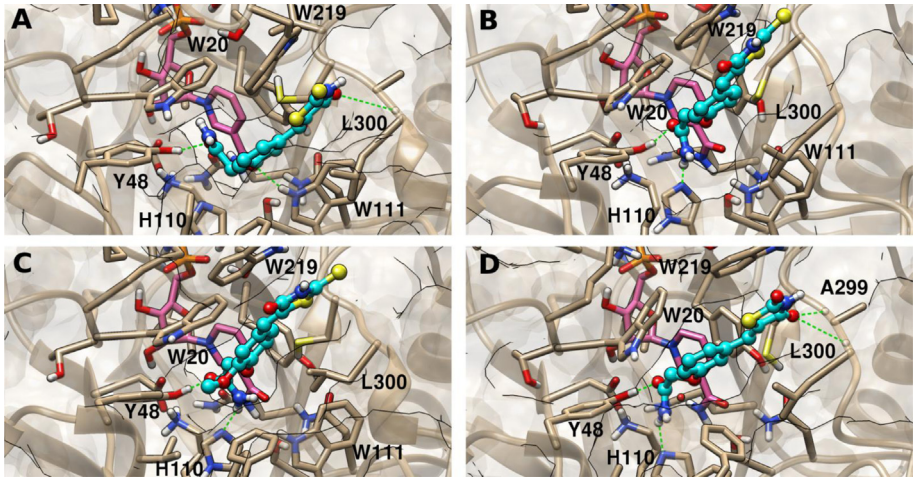

Fig. 4. Views of the binding site in modelled AR–ligand complexes after 20 ns of MD. The AMD modes for **7a** (A), **7b** (B), **7d** (C) and **6a** (D) are shown using a beige ribbon plus selected (within 5 Å from ligand) stick sidechain representation for AR, pink sticks for NADP+ and cyan ball-and-stick for ligands. For all molecules only polar hydrogens are shown. Heteroatoms and polar hydrogens are coloured according to a standard scheme (red for oxygen, blue for nitrogen, yellow for sulphur and white for hydrogen). Intermolecular H-bonds are shown as green dotted-lines. (For interpretation of the references to colour in this figure legend, the reader is referred to the web version of this article.)

2.3.4. AR–6a complex

Trajectory analysis of RING mode for AR–**6a** complex showed a different arrangement of the 2,4-thiazolidinedione moiety in comparison with the 2-thioxo-4-thiazolidinone one of **7a**. Besides the H-bonds with His110 and Trp111, shared by both compounds, the exocyclic oxygen atom in position 2 of **6a** formed an additional H-bond with Tyr48 side-chain, which, in AR–**7a** complex, is H-bonded to a resident water molecule (Fig. 3C). To exclude that **7a** can adopt this binding mode, a new MD simulation of AR–**7a** complex was carried out, by modelling the binding mode of compound **7a** on the final configuration of the AR–**6a** complex, but also in this case the model evolved toward the arrangement described above for AR–**7a**. As a result of the different heterocycle arrangements, the arylidene moiety is more flexible in AR–**6a** complex than in AR–**7a**, oscillating between the interaction with Phe122 and the loop region Ala299-Leu301, in the absence of a stable H-bond pattern involving the 3-carbamoylmethoxy group. Instead, the AMD orientations in AR–**6a** complex are similar to those already described for **7a** (Fig. 4D).

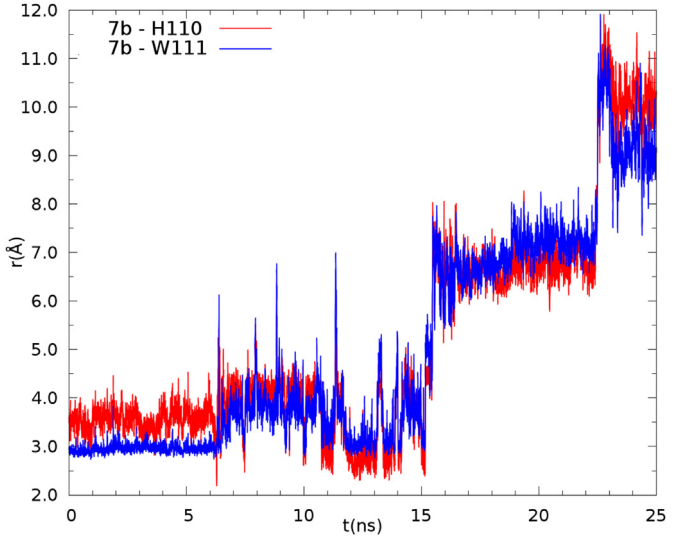

Fig. 5. Time-dependence of H-bond distances along MD simulation of the AR–7b RING binding mode. Distances (in Å) are plotted as a function of time (ns) for **7b** (N3)-AR(H110:N_{ε}) (red line) and **7b** (O4)-AR(W111:$N_{\varepsilon 1}$) (blue line) atom pairs. (For interpretation of the references to colour in this figure legend, the reader is referred to the web version of this article.)

2.3.5. AR–9d complex

As expected, **9d**, the representative inhibitor selected among compounds **9a**–**d**, bearing a negatively-charged carboxylate group in position 3, exhibited an interaction energy almost twice than that of the neutral N-unsubstituted analogue (**7d**). The ionizable group stably anchored the ligand in the anionic binding site, through stable H-bond and ionic interaction, respectively with Tyr48/His110 side-chains and the positively charged nicotinamide moiety of the cofactor. This interaction is, in principle, fully compatible with both RING-Oin and RING-Oout orientations of the 2-thioxo-4-thiazolidinone scaffold in the binding pocket. However, as shown in Table 3, RING-Oin of AR–**9d** complex was more stable by 3 kcal mol^{-1} than RING-Oout, because of the different orientation of the arylidene moiety, which in RING-Oin formed a persistent H-bond through the ether oxygen of the 4-carbamoylmethoxy group with NH backbone atom of Leu301. This interaction, in turn, stabilized a network of hydrophobic interactions involving the 3-methoxy group of the inhibitor and Ala299, Leu301 and Trp219 side-chains of AR (Fig. 6A). In RING-Oout the aforementioned stable H-bond was missing, replaced by a set of labile concurrent H-bonds, which, by increasing local positional fluctuations, also negatively affected the persistence of the hydrophobic interactions (Fig. 6B).

The most evident general trend among the different outcomes obtained by combining the results of our computational approach with the corresponding experimental activity data is the overwhelming contribution of the carboxylic group of compounds **8** and **9** to AR binding. In fact, on one hand only negligible differences in potency were observed in experimental data within compounds **9a**–**d**, and on the other hand MD simulations showed that the stability of the different AR–**9d** binding modes is relatively unaffected by the different orientation and interaction patterns of other functional groups of the inhibitor.

Conversely, both 5-arylidene-2-thioxo-4-thiazolidinones (**7**) and 5-arylidene-2,4-thiazolidinediones (**6**), which are lacking in the carboxylic acid group on N-3, are very sensitive to both the nature and position of the substituents on the aryl group, showing similar trends within each series. For neutral compounds **6** and **7** the two main binding mode classes, both the so-called RING and

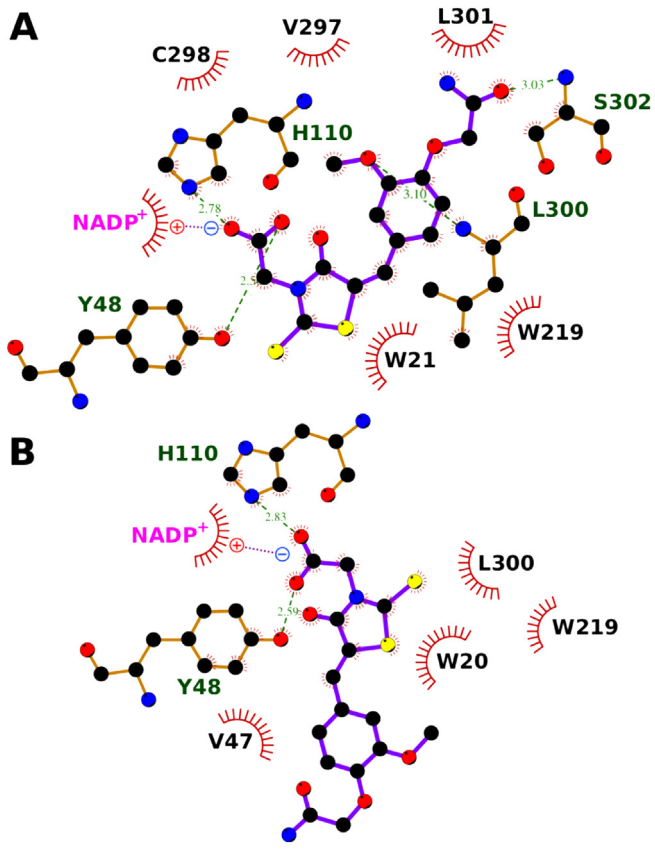

Fig. 6. Ligand–protein interactions in AR–**9d** complex models. The LigPlot+ [47] representation, enriched with the $NADP^+$–ligand ionic interaction (violet dotted line between ± charge signs), is shown for Oin (A) and Oout (B) binding modes. Ligand and protein residues involved in H-bonds (green dotted lines) are shown as ball-and-lines (with violet and brown bonds for **9d** and protein residues, respectively), while protein residues and ligand atoms forming hydrophobic contacts are surrounded by purple spoked arcs. (For interpretation of the references to colour in this figure legend, the reader is referred to the web version of this article.)

AMD orientations, were generally accessible in term of stability shown during MD simulations and protein-inhibitor energy interaction values, except for **7b**. The RING binding mode of this latter compound, which exhibited the lowest experimental activity within the series, was not stable already on a nanosecond timescale. Compound **7d**, which shares with **7b** the carbamoylmethoxy group in the para position of the arylidene group, was able to recover binding in the RING mode through the presence of the methoxy group in meta position, which mimicked part of the stabilizing interactions occurring in the corresponding complex model of **7a**, the most active inhibitor within the N-unsubstituted series.

Thus, the comparable inhibitory effectiveness of compounds **7a** and **7d**, significantly higher than that of **7b**, can easily be rationalized in terms of a stronger binding provided by RING modes (plus an eventual minor contribution from AMD) in comparison with the weaker binding associated to the sole predicted AMD mode for **7b**.

The slight differences in potency observed between compounds **7a** and **7d** can also be explained on the basis of the overwhelming contribution to binding provided by RING modes, since their predicted complex models shared substantially the same interaction pattern in AMD mode while differed in RING orientation.

The replacement of an oxygen atom with sulphur promoted a rearrangement of 2-thioxo-4-thiazolidinone ring in the anionic binding site that prevented the formation of a direct H-bond with Tyr48, instead occurring in the 2,4-thiazolidinedione series. When the interaction patterns and energies of the RING-mode complexes of **7a** and **6a** were compared in detail, it emerged that the lack of a H-bond was more than compensated by the extra-stabilization provided by the stable interaction of a water molecule with Tyr48 (H-bond) and the inhibitor (favourable electrostatic and van der Waals interactions). However, a quantitative comparison between predicted AR affinities of **7a** and **6a** is beyond the scope of the present study, since it would require both the precise evaluation of polarization effects upon oxygen/sulphur replacement, and the comparison of binding free energies between a binary and a ternary complex.

2.4. Antiinflammatory activity

In order to evaluate the effectiveness of this series of ARIs on inflammatory pathways, 2-thioxo-4-thiazolidinone derivatives **7a**, **7c**, **9a**, **9c**, and **9d** were selected as representative inhibitors among either acetic acid derivatives (compounds **9**) or N-unsubstituted analogues (compounds **7**).

The anti-inflammatory activity was evaluated in vitro on the normal human keratinocyte cell line NCTC 2544 exposed to IFN-γ and histamine, this latter used to strongly increase the IFN-γ-induced keratinocyte activation [33,34].

The tested compounds did not interfere significantly with cellular viability at the tested doses, maintaining the capability of these cells to metabolize tetrazolium salts (data not shown).

As above described, NF-kB is highly activated at sites of inflammation in diverse diseases and can induce transcription of proinflammatory cytokines, chemokines, adhesion molecules, MMPs, COX-2, and iNOS. In this study the levels of NF-kB and iNOS proteins were determined [35] and reported in Figs. 7 and 8.

Compounds **9a, 9c**, and **9d** can reduce the activation of NF-kB demonstrating to inhibit NF-kB nuclear translocation in stimulated cells compared to the control (Fig. 7). On the contrary, N-unsubstituted compound **7a** appeared to be ineffective, whereas compound **7c** reduced only slightly the activation of NF-kB. Therefore, the presence of the acetic acid group was also shown to be favourable for the reduction of NF-kB activation. Interestingly,

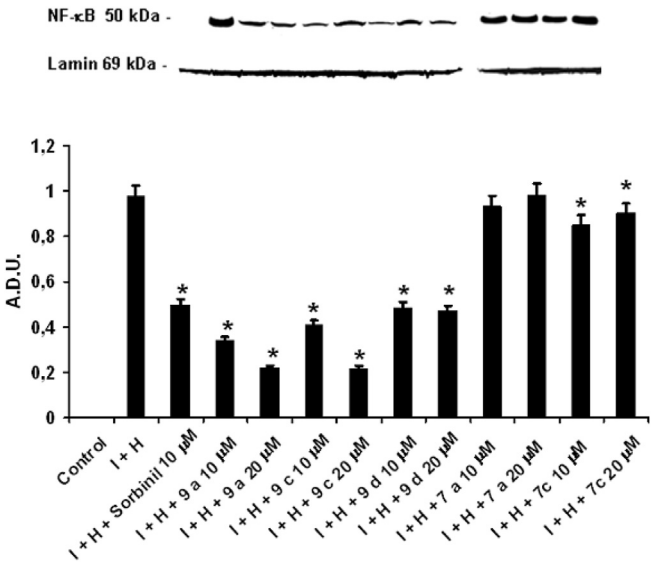

Fig. 7. Effects of 2-thioxo-4-thiazolidinone derivatives **9a**, **9c**, **9d**, **7a**, and **7c** on NF-kB activation induced by interferon-γ (I) plus histamine (H) on human keratinocytes NCTC 2544 determined by Western blot analysis. Data show the relative expression (mean ± SEM) of NF-kB calculated as arbitrary densitometric units (A.D.U.) collected from three independent experiments. $^*p < 0.05$ compared to interferon-γ (I) plus histamine (H)-induced NF-kB.

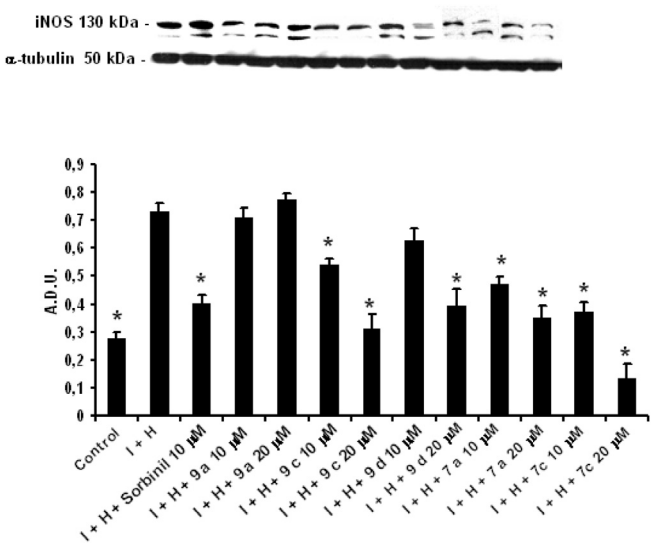

Fig. 8. Effects of derivatives **9a**, **9c**, **9d**, **7a**, and **7c** on iNOS expression induced by interferon-γ (I) plus histamine (H) on human keratinocytes NCTC 2544 determined by Western blot analysis. Data show the relative expression (mean ± SEM) of iNOS calculated as arbitrary densitometric units (A.D.U.) collected from three independent experiments. $^{*}p < 0.05$ compared to interferon-γ(I) plus histamine (H)-induced iNOS.

compounds **9a**, **9c** and **9d**, at 10 μM dose, showed activity comparable to that of sorbinil, used as reference drug (Fig. 7).

As shown in Fig. 8, iNOS expression levels by human keratinocyte cells in the culture medium decreased in a dose-dependent manner upon the treatment with the selected compounds, except for compound **9a** that resulted to be nearly ineffective. At the highest dose (20 μM), compounds **7a**, **7c** and **9c** were shown to reduce the iNOS expression up to reaching the control level.

In our experimental model compound **9c** displays the most marked anti-inflammatory activity being able, at the dose of 10 μM, to significantly reduce both NF-kB activation and iNOS expression. Similar considerations apply to compound **7c**, even though the effect on NF-kB activation is less evident. More puzzling is the behaviour of compounds **9a, 7a**, and **9d**, which are able to affect only NF-kB activation or only iNOS expression, respectively. Thus, overall an anti-inflammatory activity can be envisaged for all the tested ARIs. Moreover, it is important to note that the inhibition of the IFN-γ and histamine-stimulated production of pro-inflammatory molecules in keratinocytes NCTC 2544 by **7a**, **7c**, **9a**, **9c,** and **9d** was not due to cytotoxicity, as assessed by MTT assay. However, for a complete clarification of their mechanism of action, further study are needed, in particular by evaluating the contribution of the AR-dependent pathway to the overall inflammatory signalling in the adopted experimental model.

3. Conclusions

In this paper we report the synthesis, biological activity, and SARs of a new series of 4-thiazolidinone derivatives which differ by substitutions at N-3 and C-2 positions as well as at 5-arylidene moiety.

In vitro AR inhibitory activity indicated that the 2-thioxo-4-thiazolidinone core is more favourable for the AR affinity in comparison with the 2,4-thiazolidinedione isosteric ring.

Molecular docking studies suggested a different binding mode in the RING orientation between the two series, with a resident water molecule contributing to an extra-stabilization in the case of the 4-oxo-2-thioxothiazolidine core. A potentially relevant contribution to the better activity exhibited by the 2-thioxo-4-thiazolidinone series in comparison with the 2,4-thiazolidinedione one could be provided by polarization effects involving the sulphur atom in the former series. However an accurate evaluation of this energy term is beyond the scope of the present work, since it requires extensive quantomechanic (QM) and hybrid QM-molecular mechanics (MM) calculations, with a careful definition of the QM part of the system and of the QM/MM boundary, also keeping into account the observed occurrence of a resident water molecule only in the **7a** complex.

SARs combined with modelling studies indicated that carboxylic acid derivatives **8** and **9** have a greater binding affinity with the enzyme than N-unsubstituted counterpart **6** and **7** independent of the nature of the group in position 2. Comparing the AR inhibitory activity of N-unsubstituted compounds **6** and **7** and the corresponding N-3 acetic acid substituted analogues (compounds **8** and **9**) highlights the central role carried out by the ionisable carboxylic group that can stably anchor the ligand in the anionic binding site of the enzyme.

Interestingly, compounds **7a**, **7c**, **9a**, **9c** and **9d** also exhibited anti-inflammatory activity by reducing NF-kB activation and/or iNOS expression in cultures of human keratinocytes exposed to IFN-γ and histamine. In particular, compounds **9a** and **9c** were shown to interfere in the cellular inflammatory pathways by intervening in NF-kB activation, which is an upstream event in the inflammatory cascade. Among the selected compounds, {5-[(3-carbamoylmethoxy-4-methoxyphenyl)methylidene]-4-oxo-2-thioxothiazolidin-3-yl}acetic acid (**9c**) stood out for its submicromolar AR inhibitory efficacy joined to the ability to reduce both NF-kB activation and iNOS expression. Its interesting biological profile makes it worthy to be considered as a new lead compound. The goal of further optimization will be supported by the molecular modelling study which provided a rationalization of the observed trend in experimental affinity data of this class of ARIs and also suggested criteria to direct future drug design. Moreover, in view of the recently proposed new approach in the inhibition of AR [36] it will be relevant to assess the ability of these compounds to act as differential AR inhibitors.

4. Experimental section

4.1. Chemistry

Melting points were recorded on a Kofler hot-stage apparatus and are uncorrected. TLC controls were carried out on precoated silica gel plates (F 254 Merck). Elemental analyses (C, H, N), determined by means of a C. Erba mod. 1106 elem. Analyzer, were within ±0.4% of the theoretical values. ^{1}H and ^{13}C NMR spectra were routinely recorded at a constant temperature of 27C on a Varian Inova-200 spectrometer in $CDCl_3$ or DMSO-d_6 solution; chemical shifts δ are expressed in ppm with reference to TMS as an internal standard. Coupling constants (J) are given in hertz (Hz). ^{13}C NMR spectra were determined by Attached Proton Test (APT) experiments and the resonances were always attributed by proton-carbon heteronuclear chemical shift correlation.

Unless stated otherwise, all materials were obtained from commercial suppliers and used without further purification.

General procedure for the synthesis of 2-(formylaryloxy)acetamides **5a**–**d**, their chemical–physical ^{1}H and ^{13}C data are reported in the Supplementary material.

4.2. General procedure for the synthesis of 2-[(2,4-dioxothiazolidin-5-ylidenemethyl)phenoxy]acetamides *6a*–*d*

A mixture of 2,4-thiazolidinedione (2.3 g, 20 mmol), appropriate aldehyde **5** (20 mmol), piperidine (1.4 g, 16 mmol) and EtOH (80 ml)

was refluxed for 24–27 h. The reaction mixture was poured into H_2O acidified with AcOH to give a crude solid which was recrystallized from methanol to give pure acetamide **6**.

4.2.1. 2-[3-(2,4-Dioxothiazolidin-5ylidenemethyl)phenoxy] acetamide (**6a**)

Yield 46%; mp 272–275 °C; ^{1}H NMR (DMSO-d_6): δ 4.48 (s, 2H, CH_2O); 7.05 (dd, $J_1 = 8.0$, $J_2 = 2.0$ Hz, 1H, CH arom); 7.14 (s, 1H, CH arom); 7.19 (d, $J = 8.5$ Hz, 1H, CH arom); 7.39 (brs, 1H, NH); 7.58 (brs, 1, NH); 7.44 (t, $J = 8.0$ Hz, 1H, CH arom); 7.72 (s, 1H, CH methylidene); 12.59 (brs, 1H, NH). ^{13}C NMR (DMSO-d_6): δ 66.7 (CH_2); 115.6, 116.8, 122.8, 124.3, 130.3, 131.3 (CH arom, CH methylidene, 5-C); 134.4, 158.2 (Cq arom); 167.6, 168.0, 169.6 (CO). Anal. ($C_{12}H_{10}N_2O_4S$) calcd: C 51.79, H 3.62, N 10.07; found: C 51.69, H 3.47, N 9.97.

4.2.2. 2-[4-(2,4-Dioxothiazolidin-5-ylidenemethyl)phenoxy] acetamide (**6b**)

Yield 48%; mp 295 °C dec.; ^{1}H NMR (DMSO-d_6): δ 4.51 (s, 2H, CH_2O); 7.09 (m, 2H, CH arom); 7.39 (brs, 1H, NHCO); 7.55 (m, 3H, CH arom, NHCO); 7.74 (s, 1H, CH methylidene); 12.50 (brs, 1H, NH). ^{13}C NMR (DMSO-d_6): δ 66.6 (CH_2); 115.5, 120.6, 131.7, 131.9 (CH arom, 5-C, CH methylidene); 126.0, 159.4 (Cq arom); 167.4, 167.9, 169.3 (CO). Anal. ($C_{12}H_{10}N_2O_4S$) calcd: C 51.79, H 3.62, N 10.07; found: C 51.65, H 3.49, N 10.17.

4.2.3. 2-[5-(2,4-Dioxothiazolidin-5-ylidenemethyl)-2-methoxyphenoxy]acetamide (**6c**)

Yield 54%; mp 258 °C dec; ^{1}H NMR (DMSO-d_6): δ 3.85 (s, 3H, CH_3); 4.49 (s, 2H, CH_2O); 7.08 (d, $J = 2.0$ Hz, 1H, CH arom); 7.15 (d, $J = 8.5$ Hz, CH arom); 7.23 (dd, $J_1 = 8.5$, $J_2 = 2.0$ Hz, 1H, CH arom); 7.40 (2 brs, 2H, NH_2); 7.68 (s, 1H, CH methylidene); 12.48 (brs, 1H, NH). ^{13}C NMR (DMSO-d_6): δ 55.8 (CH_3); 67.6 (CH_2); 112.5, 114.8, 120.6, 125.1, 125.5 (CH arom, CH methylidene, 5-C); 131.8, 147.6, 151.1 (Cq arom); 167.3, 168.0, 169.5 (CO). Anal. ($C_{13}H_{12}N_2O_5S$) calcd: C 50.64, H 3.92, N 9.09; found: C 50.39, H 3.81, N 8.91.

4.2.4. 2-[4-(2,4-Dioxothiazolidin-5-ylidenemethyl)-2-methoxyphenoxy]acetamide (**6d**)

Yield 47%; mp 274 °C dec; ^{1}H NMR (DMSO-d_6): δ 3.83 (s, 3H, CH_3); 4.52 (s, 2H, CH_2O); 7.01 (d, $J = 8.5$ Hz, CH); 7.14 (dd, $J_1 = 8.5$, $J_2 = 2.0$ Hz, 1H, CH arom); 7.22 (d, $J = 2.0$ Hz, 1H, CH arom); 7.35, 7.38 (2 brs, 2H, NH_2); 7.74 (s, 1H, CH methylidene); 12.51 (brs, 1H, NH). ^{13}C NMR (DMSO-d_6): δ 55.7 (CH_3); 67.3 (CH_2); 113.7, 113.8, 121.0, 123.3, 126.5 (CH arom, CH methylidene, 5-C); 132.0, 149.1, 149.3 (Cq arom); 167.3, 167.9, 169.4 (CO). Anal. ($C_{13}H_{12}N_2O_5S$) calcd: C 50.64, H 3.92, N 9.09; found: C 50.44, H 3.85, N 8.95.

4.3. General procedure for the synthesis of 2-[(4-oxo-2-thioxothiazolidin-5-ylidenemethyl)phenoxy]acetamides **7a–d**

A mixture of 2-thioxo-4-thiazolidinone (0.8 g, 6 mmoli), appropriate aldehyde **5** (6 mmol), sodium acetate (1.82 g, 22.2 mmol) and glacial acetic acid (15 ml) was refluxed for 4–6 h. The reaction mixture was poured into H_2O and filtered off. The solid was recrystallized from methanol to give pure acetamide **7**.

4.3.1. 2-[3-(4-Oxo-2-thioxothiazolidin-5-ylidenemethyl)phenoxy] acetamide (**7a**)

Yield 79%; mp 272–275 °C; ^{1}H NMR (DMSO-d_6): δ 4.49 (s, 2H, CH_2O); 7.08 (dd, $J_1 = 8.0$, $J_2 = 2.0$ Hz, 1H, CH arom); 7.13 (m, 1H, CH arom); 7.19 (d, $J = 8.0$ Hz, 1H, CH arom); 7.40 (brs, 1H, CONH); 7.45 (t, $J = 8.0$ Hz, 1H, CH arom); 7.58 (s, 1H, CH methylidene); 7.60 (brs, 1H, CONH); 13.82 (brs, 1H, NH). ^{13}C NMR (DMSO-d_6): δ 66.7 (CH_2); 116.0, 117.2, 123.4, 125.9, 130.5, 131.3 (CH arom, CH methylidene, 5-C); 134.2, 158.2 (Cq arom); 169.3, 169.5 (CO); 195.6 (CS). Anal. ($C_{12}H_{10}N_2O_3S_2$) calcd: C 48.97, H 3.42, N 9.52; found: C 48.76, H 3.55, N 9.34.

4.3.2. 2-[4-(4-Oxo-2-thioxothiazolidin-5-ylidenemethyl)phenoxy] acetamide (**7b**)

Yield 72%; mp 292 °C dec; ^{1}H NMR (DMSO-d_6): δ 4.52 (s, 2H, CH_2O); 7.10 (m, 2H, CH arom); 7.40 (brs, 1H, NHCO); 7.56 (m, 2H, CH arom); 7.57 (brs, 1H, NHCO); 7.59 (s, 1H, CH methylidene); 13.73 (brs, 1H, NH). ^{13}C NMR (DMSO-d_6): δ 66.6 (CH_2); 115.7, 122.6, 125.9, 131.7 (CH arom, CH methylidene, 5-C); 132.5, 159.8 (Cq arom); 169.3, 169.4 (CO); 195.5 (CS). Anal. ($C_{12}H_{10}N_2O_3S_2$) calcd: C 48.97, H 3.42, N 9.52; found: C 48.75, H 3.62, N 9.45.

4.3.3. 2-[2-Methoxy-5-(4-oxo-2-thioxothiazolidin-5-ylidenemethyl)phenoxy]acetamide (**7c**)

Yield 69%; mp 258 °C dec. ^{1}H NMR (DMSO-d_6): δ 3.86 (s, 3H, CH_3); 4.50 (s, 2H, CH_2O); 7.08 (d, $J = 1.5$ Hz, 1H, CH arom); 7.16 (d, $J = 8.5$ Hz, CH arom); 7.25 (dd, $J_1 = 8.5$, $J_2 = 1.5$ Hz, 1H, CH arom); 7.40 (2 brs, 2H, NH_2); 7.55 (s, 1H, CH methylidene); 13.73 (brs, 1H, NH). ^{13}C NMR (DMSO-d_6): δ 55.8 (CH_3); 67.6 (CH_2); 112.6, 115.1, 122.5, 125.5, 125.9 (CH arom, CH methylidene, 5-C); 131.9, 147.6, 151.5 (Cq arom); 169.4, 169.5 (CO); 195.5 (CS). Anal. ($C_{13}H_{12}N_2O_4S_2$) calcd: C 48.14, H 3.73, N 8.64; found: C 48.05, H 3.62, N 8.55.

4.3.4. 2-[2-Methoxy-4-(4-oxo-2-thioxothiazolidin-5-ylidenemethyl)phenoxy]acetamide (**7d**)

Yield 44%; mp 275 °C dec. ^{1}H NMR (DMSO-d_6): δ 3.84 (s, 3H, CH_3); 4.53 (s, 2H, CH_2O); 7.02 (d, $J = 8.0$ Hz, 1H, CH arom); 7.16 (dd, $J_1 = 8.0$, $J_2 = 2.0$ Hz, CH arom); 7.20 (d, $J = 2.0$ Hz, 1H, CH arom); 7.36, 7.39 (2 brs, 2H, NH_2); 7.60 (s, 1H, CH methylidene); 13.75 (brs, 1H, NH). ^{13}C NMR (DMSO-d_6): δ 55.7 (CH_3); 67.3 (CH_2); 113.8, 113.9, 122.8, 124.1, 126.4 (CH arom, CH methylidene, 5-C); 132.0, 149.2, 149.7 (Cq arom); 169.3, 169.4 (CO); 195.5 (CS). Anal. ($C_{13}H_{12}N_2O_4S_2$) calcd: C 48.14, H 3.73, N 8.64; found: C 47.95, H 3.65, N 8.39.

4.4. General procedure for the synthesis of (5-arylidene-2,4-dioxothiazolidin-3-yl)acetic acids **8a–d**

A mixture of 2,4-thiazolidinedione (1 g, 8.5 mmol), methyl bromoacetate (2.6 g, 17 mmol) and potassium carbonate (2.35 g, 17 mmol) was refluxed for 24 h; then the solvent was evaporated under reduced pressure. The residue was washed with methanol to provide (2,4-dioxothiazolidin-3-yl)acetic acid methyl ester as oil. A mixture of (2,4-dioxothiazolidin-3-yl)acetic acid methyl ester (0.8 g, 4.23 mmol) glacial AcOH (17 ml) and HCl 2 N (4.2 ml) was refluxed for 90 min. After evaporation in vacuo, the crude mixture was refluxed again with AcOH (17 ml) and HCl (4.2 ml) for 90 min. After evaporation to dryness in vacuo, the crude oil was washed with H_2O and then with ethanol to provide pure (2,4-dioxothiazolidin-3-yl)acetic acid (**10**) as oil [22]. A mixture of (2,4-dioxothiazolidin-3-yl)acetic acid (**10**) (0.5 g, 2.86 mmol), appropriate aldehyde 5 (2.86 mmol), piperidine (0.19 g, 2.29 mmol) and EtOH (50 ml) was refluxed for 24 h. The reaction mixture was poured into H_2O acidified with AcOH to give a crude solid which was recrystallized from methanol to give pure acid **8**.

4.4.1. {5-[(3-Carbamoylmethoxyphenyl)methylidene]-2,4-dioxothiazolidin-3-yl}acetic acid (**8a**)

Yield 58%; mp 251–253 °C; ^{1}H NMR (DMSO-d_6): δ 4.37 (s, 2H, NCH_2); 4.49 (s, 2H, OCH_2); 7.08–7.49 (m, 4H, CH arom); 7.59 (brs, 2H, $CONH_2$); 7.94 (s, 1H, CH methylidene). ^{13}C NMR (DMSO-d_6): δ 42.3 (NCH_2); 66.7 (OCH_2); 115.8, 117.4, 123.0, 130.5, 133.6 (CH arom, CH methylidene); 121.2 (C-5); 134.0, 158.2 (Cq arom); 164.9, 166.9, 167.9, 169.5 (CO). Anal. ($C_{14}H_{12}N_2O_6S$) calcd: C 50.00, H 3.60, N 8.33; found: C 49.78, H 3.44, N 8.11.

4.4.2. {5-[(4-Carbamoylmethoxyphenyl)methylidene]-2,4-dioxothiazolidin-3-yl}acetic acid (**8b**)

Yield 53%; mp 275–276 °C; ^{1}H NMR (DMSO-d_6): δ 4.34 (s, 2H, NCH_2) 4.53 (s, 2H, OCH_2); 7.11 (m, 2H, CH arom); 7.62 (m, 2H, CH arom); 7.41 (brs, 2H, $CONH_2$); 7.94 (s, 1H, CH methylidene). ^{13}C NMR (DMSO-d_6): δ 42.3 (NCH_2); 67.0 (OCH_2); 114.5, 124.9, 133.9 (CH arom, CH methylidene), 117.9, 125.9, 149.5 (Cq arom, 5-C); 165.0, 167.0, 167.5, 169.4 (CO). Anal. ($C_{14}H_{12}N_2O_6S$) calcd: C 50.00, H 3.60, N 8.33; found: C 49.81, H 3.50, N 8.27.

4.4.3. {5-[(3-Carbamoylmethoxy-4-methoxyphenyl)methylidene]-2,4-dioxothiazolidin-3-yl}acetic acid (**8c**)

Yield 51%; mp 235–237 °C; ^{1}H NMR (DMSO-d_6): δ 3.85 (s, 3H, CH_3); 4.35 (s, 2H, NCH_2); 4.50 (s, 2H, OCH_2); 7.13–7.31 (m, 3H, CH arom); 7.43 (brs, 2H, $CONH_2$); 7.88 (s, 1H, CH methylidene). ^{13}C NMR (DMSO-d_6): δ 42.2 (NCH_2); 55.8 (CH_3); 67.6 (OCH_2); 112.6, 114.9, 125.5, 133.9 (CH arom, CH methylidene); 117.7, 125.2, 147.6, 151.5 (Cq arom, 5-C); 165.1, 167.0, 168.0, 169.5 (CO). Anal. ($C_{15}H_{14}N_2O_7S$) calcd: C 49.18, H 3.85, N 7.65; found: C 49.29, H 3.67, N 7.39.

4.4.4. {5-[(4-Carbamoylmethoxy-3-methoxyphenyl)methylidene]-2,4-oxothiazolidin-3-yl}acetic acid (**8d**)

Yield 50%; mp 240–242 °C; ^{1}H NMR (DMSO-d_6): δ 3.86 (s, 3H, CH_3), 4.38 (s, 2H, NCH_2) 4.55 (s, 2H, OCH_2); 7.02–7.41 (m, 5H, CH arom, $CONH_2$); 7.95 (s, 1H, CH methylidene). ^{13}C NMR (DMSO-d_6): δ 42.3 (NCH_2), 55.7 (CH_3), 67.3 (OCH_2), 113.8, 114.0, 123.6, 134.0 (CH arom, CH methylidene), 118.1, 126.3, 149.2, 149.7 (Cq arom, 5-C), 165.1, 167.0, 168.0, 169.3 (CO). Anal. ($C_{15}H_{14}N_2O_7S$) calcd: C 49.18, H 3.85, N 7.65; found: C 49.31, H 3.72, N 7.78.

4.5. General procedure for the synthesis of (5-arylidene-4-oxo-2-thioxothiazolidin-3-yl)acetic acids **9a–d**

A mixture of (4-oxo-2-thioxothiazolidin-3-yl)acetic acid (1.15 g, 6 mmol), appropriate aldehyde **5** (6 mmol), sodium acetate (3.69 g, 45 mmol) and glacial acetic acid (30 ml) was refluxed for 2–5 h. The reaction mixture was poured into H_2O and filtered off. The solid was recrystallized from methanol to give pure acid **9**.

4.5.1. {5-[(3-Carbamoylmethoxyphenyl)methylidene]-4-oxo-2-thioxothiazolidin-3-yl}acetic acid (**9a**)

Yield 75%; mp 254–256 °C; ^{1}H NMR (DMSO-d_6): δ 4.51 (s, 2H, NCH_2) 4.74 (s, 2H, OCH_2); 7.13 (dd J_1 = 8.0, J_2 = 2.0 Hz, 1H, CH arom); 7.22 (m, 1H, CH arom); 7.27 (d J = 8.0 Hz, 1H, CH arom); 7.41 (brs, 1H, CONH); 7.49 (t J = 8.0 Hz, 1H, CH arom); 7.62 (brs, 1H, CONH). 7.84 (s, 1H, CH methylidene). ^{13}C NMR (DMSO-d_6): δ 45.0 (NCH_2); 66.7 (OCH_2); 116.3, 117.7, 122.3, 123.6, 130.6, 133.7 (CH arom, CH methylidene, 5-C); 134.0, 158.3 (Cq arom); 166.3, 167.2, 169.5 (CO); 193.3 (CS). Anal. ($C_{14}H_{12}N_2O_5S_2$) calcd: C 47.72, H 3.43, N 7.95; found: C 47.59, H 3.35, N 7.79.

4.5.2. {5-[(4-Carbamoylmethoxyphenyl)methylidene]-4-oxo-2-thioxothiazolidin-3-yl}acetic acid (**9b**)

Yield 64%; mp 275–276 °C; ^{1}H NMR (DMSO-d_6): δ 4.54 (s, 2H, NCH_2); 4.72 (s, 2H, OCH_2); 7.12 (m, 2H, CH arom); 7.41 (brs, 1H, CONH); 7.59 (brs, 1H, CONH); 7.65 (m, 2H, CH arom); 7.84 (s, 1H, CH methylidene). ^{13}C NMR (DMSO-d_6): δ 45.0 (NCH_2); 66.7 (OCH_2); 115.8, 132.9 (CH arom); 118.8, 125.8, 133.9, 160.2 (5-C, CH methylidene, Cq arom); 166.4, 167.3, 169.2 (CO); 193.1 (CS). Anal. ($C_{14}H_{12}N_2O_5S_2$) calcd: C 47.72, H 3.43, N 7.95; found: C 47.45, H 3.29, N 7.66.

4.5.3. {5-[(3-Carbamoylmethoxy-4-methoxyphenyl)methylidene]-4-oxo-2-thioxothiazolidin-3-yl}acetic acid (**9c**)

Yield 68%; mp 261–263 °C; ^{1}H NMR (DMSO-d_6): δ 3.87 (s, 3H, CH_3); 4.52 (s, 2H, NCH_2); 4.71 (s, 2H, OCH_2); 7.15 (d, J = 2.0 Hz, 1H, CH arom); 7.19 (d, J = 8.5 Hz, 1H, CH arom); 7.33 (dd, J_1 = 8.5, J_2 = 2.0 Hz, 1H, CH arom); 7.42 (brs, 2H, $CONH_2$); 7.79 (s, 1H, CH methylidene). ^{13}C NMR (DMSO-d_6): δ 45.1 (NCH_2); 55.9 (CH_3); 67.6 (OCH_2); 112.7, 115.3, 118.8, 125.3, 126.4 (CH arom, CH methylidene, 5-C); 134.1, 147.7, 151.9 (Cq arom); 166.4, 167.3, 169.5 (CO); 193.1 (CS). Anal. ($C_{15}H_{14}N_2O_6S_2$) calcd: C 47.11, H 3.69, N 7.33; found: C 46.96, H 3.53, N 7.19.

4.5.4. {5-[(4-Carbamoylmethoxy-3-methoxyphenyl)methylidene]-4-oxo-2-thioxothiazolidin-3-yl}acetic acid (**9d**)

Yield 62%; mp 238–240 °C; ^{1}H NMR (DMSO-d_6): δ 3.86 (s, 3H, CH_3); 4.55 (s, 2H, NCH_2); 4.70 (s, 2H, OCH_2); 7.04 (d, J = 8.0 Hz, 1H, CH arom); 7.24 (dd, J_1 = 8.5, J_2 = 2 Hz, 1H, CH arom); 7.28 (d, J = 2.0 Hz, 1H, CH arom); 7.37, 7.39 (2 brs, 2H, $CONH_2$); 7.84 (s, 1H, CH methylidene). ^{13}C NMR (DMSO-d_6): δ 45.0 (NCH_2); 55.7 (CH_3); 67.2 (OCH_2); 113.8, 114.2, 119.1, 124.6, 126.3 (CH arom, CH methylidene, 5-C); 134.3, 149.3, 150.1 (Cq arom); 166.3, 167.3, 169.2 (CO); 193.1 (CS). Anal. ($C_{15}H_{14}N_2O_6S_2$) calcd: C 47.11, H 3.69, N 7.33; found: C 46.89, H 3.48, N 7.19.

4.6. Aldose reductase inhibition assay

AR was purified to electrophoretic homogeneity from bovine lenses as previously described [32]. The purified enzyme (specific activity 1.2 U/mg) was stored at 4 °C in 10 mM sodium phosphate buffer pH 7.0 containing 2 mM dithiothreitol. The enzymatic activity was measured at 37 °C following the decrease of absorbance at 340 nm. The assay mixture (finale volume 0.7 ml) contained, in 0.25 M sodium phosphate buffer pH 6.8, 4.67 mM D,L-glyceraldehyde, 0.11 mM NADPH, 0.38 M ammonium sulphate and 0.5 mM EDTA. One Unit of enzyme activity refers to the amount of enzyme that catalyses the oxidation of 1 μmol/min of NADPH in the above conditions.

Compounds tested as ARIs were dissolved at proper concentrations in DMSO and added to the above described assay mixture containing 5 mU of purified AR; the DMSO concentration in all the assays was kept constant at 1% (v/v). IC_{50} values (the concentration of compound required to determine a 50% inhibition of the AR activity) was determined by non linear regression analysis by fitting the data to the equation describing one site competition in a log dose–inhibition curve. For each curve, at least five different concentrations of inhibitor were analysed. The 95% confidence limits (95% C) were calculated using GraphPad Prism software.

4.7. Molecular docking – methods

Docking studies were performed with AutoDockVina 1.1.2 [37]. The crystallographic structures of AR (PDB entries 1PWM, 1US0 and 2FZD) and ligands were processed with AutoDock Tools (ADT) package version 1.5.6rc1 [38] to merge non polar hydrogens, calculate Gasteiger charges and select rotatable side-chain bonds. Grid dimensions of 22.5 × 22.5 × 22.5 Å, centred in the ligand binding pocket, were used for docking evaluation. Flexibility was allowed for all rotatable bond of docked ligands and selected residue side-chains in protein binding site, namely Trp20 and Leu300. For each target structure two docking settings were used, one with fully-rigid protein and the other with flexible Trp20 and Leu300 side-chains, thus leading to a total of six runs (three-protein scaffolds by two side-chain flexibility options) per each selected compound. The best ranking inhibitor/enzyme complexes obtained in each docking run were analysed by visual inspection, discarding

from the subsequent MD refinement either the poses not predicting direct favourable interactions (i.e. H-bonds) with at least one residue in the anionic binding site, or those poses that, after classification in families (see molecular modelling section), exhibited only a subset of favourable interactions of the closest subfamily. Representative complexes for each ligand were completed by addition of all hydrogen atoms and underwent energy minimization and then molecular dynamics (MD) simulations with ACEMD program [39], using ff12SB version of AMBER force field [40] for the protein and gaff parameters [41] for the ligands. Whenever substantial rearrangement during the MD refinement significantly affected the AR–inhibitor interaction pattern, the new ligand orientation was considered as representative of a new pose subfamily. Thus, the corresponding complex structures were built and refined also for all the other inhibitors that could form appreciable interactions according to the new binding mode.

Ligand geometries were fully optimized using GAMESS program [42] at the Hartree–Fock level with STO-3G basis set. The partial atomic charges for the ligands were derived using the RESP procedure of restrained fit to the HF/6-31G*/STO-3G electrostatic potential [43].

To perform molecular dynamics (MD) simulation in solvent, each complex was confined in water boxes using tleap module of AmberTools12 program [44] with a minimum distance between solute and box surfaces of 10 Å, filled with TIP3P water molecules and counterions (Na^+) to neutralize the system. The solvated systems were then energy minimized through 1000 steps with solute atoms restrained to their starting positions using a force constant of 10 kcal $mol^{-1}Å^{-1}$ prior to MD simulations. After this, the molecules underwent 150 ps at 300 K gradually decreasing the force constant for positional restraints on solute atoms from 100 to 1 kcal $mol^{-1}Å^{-1}$ at constant pressure. Production MD simulations were carried out at constant temperature (300 K) and pressure (1 atm) for 20 up to 25 ns with a time-step of 1 fs. Bonds involving hydrogens were constrained using the SHAKE algorithm [45]. Particle Mesh Ewald method was used to evaluate electrostatic interactions with a cutoff of 9.0 Å; the same cutoff was used for van der Waals interactions.

4.8. Evaluation of anti-inflammatory activity in vitro

4.8.1. Cell cultures and treatments

Keratinocyte cell line NCTC 2544 was provided by Interlab Cell Line Collection (Genoa, Italy) and routinely maintained in Minimum Essential Medium (MEM) (Sigma–Aldrich, Italy) supplemented with 10% foetal calf serum, 100 U/ml penicillin, and 100 μg/ml streptomycin, and incubated at 37 °C in a humidified, 95% air/5% CO_2 atmosphere. The medium was changed every 2–3 days. For experiments, 24 h before the cells were trypsinized, counted in a haemocytometer, and plated in 100 mm Petri-dishes (1.5×10^6/10 ml/well for Western blot). Experimental keratinocytes were stimulated or not (untreated controls) with 200 U/ml of IFN-γ and 10^{-4} M of histamine, used to reproduce the mechanisms involved in the pathogenesis of inflammatory processes, in the presence of different concentrations (10 and 20 μM) of the compounds **9a**, **9c**, **9d**, **7a**, and **7c**. After 48 h, each sample was tested for expression of NF-kB and iNOS.

4.8.2. Cell viability assay

The cytotoxic effect of the tested substances was evaluated by a cell viability test based on the cleavage of 3-(4,5-dimethylthiazol-2-yl)-2.5-diphenyltetrazolium bromide (MTT) by mitochondrial dehydrogenases of metabolically active cells [46].

4.8.3. Western blot

The expression of NF-kB and iNOS was evaluated by Western blot analysis. Briefly, the untreated and treated NCTC 2544 cells were washed twice with ice-cold PBS and resuspended with lysis buffer (M-PER® Mammalian Protein Extraction Reagent, Thermo scientific, PIERCE Biotechnology) supplemented with a cocktail of protease inhibitor (complete, Mini, Protease Inhibitor Cocktail Tablets, Roche) according to manufacturer's instructions. Fifty micrograms of total protein, present in the supernatant, was loaded on each lane and separated by 4–12% Novex Bis-Tris gel electrophoresis (NuPAGE, Invitrogen, Italy). Proteins were then transferred to nitrocellulose membranes (Invitrogen, Italy) in a wet system. The transfer of proteins was verified by staining the nitrocellulose membranes with Ponceau S and the Novex Bis-Tris gel with Brilliant blue R. The membranes were blocked in Tris buffered saline containing 0.01% Tween-20 (TBST) and 5% non-fat dry milk at 4 °C overnight. Polyclonal anti–NF–kB (subunit 50 kDa; nuclear activated form of NF-kB) (AB1602, Merck Millipore) (1:50,000 dilution), -NOS2 (N-20, sc-651, Santa Cruz Biotechnology) (1:300 dilution), and -α tubulin (T9026; Sigma–Aldrich) (1:5000 dilution) antibodies were diluted in TBST and the membranes incubated for 2 h at room temperature. Antibodies were detected with horseradish peroxidase conjugated secondary antibody using the enhanced chemiluminescence detection Supersignal West Pico Chemiluminescent Substrate (Pierce Chemical Co., Rockford, IL). The signal intensity of primary antibody binding was quantitatively analysed with ImageJ software and was normalized to a loading control α-tubulin. Values were expressed as arbitrary densitometric units (A.D.U.) corresponding (proportional) to signal intensity.

4.8.4. Statistical analysis

Each experiment was repeated at least three times in triplicate and the mean ± SEM for each value was calculated. Statistical analysis of results [Student's *t*-test for paired and unpaired data; variance analysis (ANOVA)] was performed using the statistical software package SYSTAT, version 11 (Systat Inc., Evanston IL, USA). A difference was considered significant at $p < 0.05$.

Acknowledgements

Work supported in part by University of Messina.

Appendix A. Supplementary data

Supplementary data related to this article can be found at http://dx.doi.org/10.1016/j.ejmech.2014.05.003.

References

[1] M. Brownlee, Biochemistry and molecular cell biology of diabetic complications, Nature 414 (2001) 813–820.
[2] L. Costantino, G. Rastelli, M.C. Gamberini, D. Barlocco, Pharmacological approaches to the treatment of diabetic complications, Exp. Opin. Ther. Patents 10 (2000) 1245–1262.
[3] P. Alexiou, K. Pegklidou, M. Chatzopoulou, I. Nicolaou, V.J. Demopoulos, Aldose reductase enzyme and its implication to major health problems of the 21th century, Curr. Med. Chem. 16 (2009) 734–752.
[4] S.K. Srivastava, K.V. Ramana, A. Bhatnagar, Role of aldose reductase and oxidative damage in diabetes and the consequent potential for therapeutic options, Endocr. Rev. 26 (2005) 380–392.
[5] A. Del Corso, M. Cappiello, U. Mura, From a dull enzyme to something else: facts and perspectives regarding aldose reductase, Curr. Med. Chem. 15 (2008) 1452–1461.
[6] N. Hotta, Y. Akanuma, R. Kawamori, K. Matsuoka, Y. Oka, M. Shichiri, T. Toyota, M. Nakashima, I. Yoshimura, N. Sakamoto, Y. Shigeta, Long-term clinical effects of Epalrestat, an aldose reductase inhibitor, on diabetic peripheral neuropathy, Diabetes Care 29 (2006) 1538–1544.
[7] N. Hotta, T. Toyota, K. Matsuoka, Y. Shigeta, R. Kikkawa, T. Kaneko, A. Takahashi, K. Sugimura, Y. Koike, J. Ishii, N. Sakamoto, Clinical efficacy of

Fidarestat, a novel aldose reductase inhibitor, for diabetic peripheral neuropathy, Diabetes Care 24 (2001) 1776–1782.
[8] R. Maccari, R. Ottanà, 2,4-Thiazolidinedione and 2-thioxo-4-thiazolidinone derivatives as aldose reductase inhibitors in the search for drugs to prevent long-term diabetes complications, in: M. Stefek (Ed.), Advances in Molecular Mechanisms and Pharmacology of Diabetic Complications, Transworld Research Network, Kerala, 2010, pp. 219–245.
[9] S. Miyamoto, Molecular modeling and structure-based drug discovery studies of aldose reductase inhibitors, Chem.-Bio. Inform. J. 2 (2002) 74–85.
[10] S. Suzen, E. Buyukbingol, Recent studies of aldose reductase enzyme inhibition for diabetic complications, Curr. Med. Chem. 10 (2003) 1329–1352.
[11] S.K. Srivastava, U.C.S. Yadav, A.B.M. Reddy, A. Saxena, R. Tammali, M. Shoeb, N.H. Ansari, A. Bhatnagar, M.J. Petrash, S. Srivastava, K.V. Ramana, Aldose reductase inhibition suppresses oxidative stress-induced inflammatory disorders, Chem. Biol. Interact. 191 (2011) 330–338.
[12] S. Miyamoto, I.M. Verma, Rel/NF-kappa B/I kappa B story, Adv. Cancer Res. 66 (1995) 255–292.
[13] A.S. Baldwin Jr., The NF-kappa B and I kappa B proteins: new discoveries and insights, Annu. Rev. Immunol. 14 (1996) 649–683.
[14] X. Teng, H. Zhang, C. Snead, J.D. Catravas, Molecular mechanism of iNOS induction by IL-1β and INF-γ in rat aortic smooth muscle cells, Am. J. Physiol. Cell Physiol. 282 (2002) C144–C152.
[15] K.V. Ramana, S.K. Srivastava, Aldose reductase: a novel therapeutic target for inflammatory pathologies, Int. J. Biochem. Cell Biol. 42 (2010) 17–20.
[16] K.V. Ramana, Aldose reductase: new insights for an old enzyme, BioMol. Concept 2 (2011) 103–114.
[17] K.V. Ramana, S.K. Srivastava, Mediation of aldose reductase in lipopolysaccharide-induced inflammatory signals in mouse peritoneal macrophages, Cytokine 36 (2006) 115–122.
[18] M. Shoeb, K.V. Ramana, S.K. Srivastava, Aldose reductase inhibition enhances TRAIL-induced human colon cancer cell apoptosis through AKT/FOXO3a-dependent upregulation of death receptors, Free Radic. Biol. Med. 63 (2013) 280–290.
[19] N.-H. Son, R. Ananthakrishnan, S. Yu, R.S. Khan, H. Jiang, R. Ji, H. Akashi, Q. Li, K. O'Shea, S. Homma, I.J. Goldberg, R. Ramasamy, Cardiomyocyte aldose reductase causes heart failure and impairs recovery from ischemia, PLoS One 7 (2012) e46549.
[20] Y.C. Hwang, M. Kaneko, S. Bakr, H. Liao, Y. Lu, E.R. Lewis, S. Yan, S. Ii, M. Itakura, L. Rui, H. Skopicki, S. Homma, A.M. Schmidt, P.J. Oates, M. Szabolcs, R. Ramasamy, Central role for aldose reductase pathway in myocardial ischemic injury, FASEB J. 18 (2004) 1192–1199.
[21] C.A. Gleissner, E. Galkina, J.L. Nadler, K. Ley, Mechanisms by which diabetes increases cardiovascular disease, Drug Discov. Today Dis. Mech. 4 (2007) 131–140.
[22] R. Maccari, R. Ottanà, C. Curinga, M.G. Vigorita, D. Rakowitz, T. Steindl, T. Langer, Structure–activity relationships and molecular modelling of 5-arylidene-2,4-thiazolidinediones active as aldose reductase inhibitors, Bioorg. Med. Chem. 13 (2005) 2809–2823.
[23] R. Maccari, R. Ottanà, R. Ciurleo, M.G. Vigorita, D. Rakowitz, T. Steindl, T. Langer, Evaluation of in vitro aldose redutase inhibitory activity of 5-arylidene-2,4-thiazolidinediones, Bioorg. Med. Chem. Lett. 17 (2007) 3886–3893.
[24] R. Maccari, R. Ottanà, R. Ciurleo, D. Rakowitz, B. Matuszczak, C. Laggner, T. Langer, Synthesis, induced-fit docking investigations, and in vitro aldose reductase inhibitory activity of non-carboxylic acid containing 2,4-thiazolidinedione derivatives, Bioorg. Med. Chem. 16 (2008) 5840–5852.
[25] R. Maccari, R. Ciurleo, M. Giglio, M. Cappiello, R. Moschini, A. Del Corso, U. Mura, R. Ottanà, Identification of new non-carboxylic acid containing inhibitors of aldose reductase, Bioorg. Med. Chem. 18 (2010) 4049–4055.
[26] R. Ottanà, R. Maccari, M. Giglio, A. Del Corso, M. Cappiello, U. Mura, S. Cosconati, L. Marinelli, E. Novellino, S. Sartini, C. La Motta, F. Da Settimo, Identification of 5-arylidene-4-thiazolidinone derivatives endowed with dual activity as aldose reductase inhibitors and antioxidant agents for the treatment of diabetic complications, Eur. J. Med. Chem. 46 (2011) 2797–2806.
[27] R. Maccari, A. Del Corso, M. Giglio, R. Moschini, U. Mura, R. Ottanà, In vitro evaluation of 5-arylidene-2-thioxo-4-thiazolidinones active as aldose reductase inhibitors, Bioorg. Med. Chem. Lett. 21 (2011) 200–203.
[28] G. Bruno, L. Costantino, C. Curinga, R. Maccari, F. Monforte, F. Nicolò, R. Ottanà, M.G. Vigorita, Synthesis and aldose reductase inhibitory activity of 5-arylidene-2,4-thiazolidinediones, Bioorg. Med. Chem. 10 (2002) 1077–1084.
[29] A. Urzhumtsev, F. Tete-Favier, A. Mitschler, J. Barbanton, P. Barth, L. Urzhumtseva, J.F. Biellmann, A.D. Podjarny, D. Moras, A "specificity" pocket inferred from the crystal structures of the complexes of aldose reductase with the pharmaceutically important inhibitors tolrestat and sorbinil, Structure 5 (1997) 601–612.
[30] S.Z. Schade, S.L. Early, T.R. Williams, F.J. Kezdy, R.L. Heinrikson, C.E. Grimshaw, C.C. Dioughty, Sequence analysis of bovine lens aldose reductase, J. Biol. Chem. 265 (1990) 3628–3635.
[31] R. Ottanà, R. Maccari, M.L. Barreca, G. Bruno, A. Rotondo, A. Rossi, G. Chiricosta, R. Di Paola, L. Sautebin, S. Cuzzocrea, M.G. Vigorita, 5-Arylidene-2-imino-4-thiazolidinones: design and synthesis of novel anti-inflammatory agents, Bioorg. Med. Chem. 13 (2005) 4243–4252.
[32] A. Del Corso, D. Barsacchi, M. Giannessi, M.G. Tozzi, M. Camici, J.L. Houben, M. Zandomeneghi, U. Mura, Bovine lens aldose reductase: tight binding of the pyridine coenzyme, Arch. Biochem. Biophys. 283 (1990) 512–518.
[33] H. Koizomi, A. Ohkawara, H2 histamine receptor-mediated increase in intracellular Ca^{2+} in cultured human keratinocytes, J. Dermatol. Sci. 21 (1999) 137–142.
[34] N. Kanda, S. Watanabe, Histamine enhances the production of nerve growth factor in human keratinocytes, J. Invest. Dermatol. 121 (2003) 570–577.
[35] V. Cardile, M. Libra, S. Caggia, G. Frasca, K. Umezawa, F. Stivala, M.C. Mazzarino, Y. Bevelacqua, M. Coco, G. Malaponte, Dehydroxymethylepoxyquinomicin, a novel nuclear factor-kappaB inhibitor, prevents inflammatory injury induced by interferon-gamma and histamine in NCTC 2544 keratinocytes, Clin. Exp. Pharmacol. Physiol. 37 (2010) 679–683.
[36] A. Del Corso, F. Balestri, E. Di Bugno, R. Moschini, M. Cappiello, S. Sartini, C. La Motta, F. Da Settimo, U. Mura, A new approach to control the enigmatic activity of aldose reductase, PLoS One 8 (2013) e74076.
[37] O. Trott, A.J. Olson, AutoDock Vina: improving the speed and accuracy of docking with a new scoring function, efficient optimization and multithreading, J. Comput. Chem. 31 (2010) 455–461.
[38] G.M. Morris, R. Huey, W. Lindstrom, M.F. Sanner, R.K. Belew, D.S. Goodsell, A.J. Olson, Autodock4 and AutoDockTools4: automated docking with selective receptor flexibility, J. Comput. Chem. 30 (2009) 2785–2791.
[39] M. Harvey, G. Giupponi, G. De Fabritiis, ACEMD: accelerated molecular dynamics simulations in the microseconds timescale, J. Chem. Theory Comput. 5 (2009) 1632–1640.
[40] V. Hornak, R. Abel, A. Okur, B. Strockbine, A. Roitberg, B. Strockbine, A. Roitberg, C. Simmerling, Comparison of multiple AMBER force fields and development of improved protein backbone parameters, Proteins 65 (2006) 712–725.
[41] J. Wang, R.M. Wolf, J.W. Caldwell, P.A. Kollman, D.A. Case, Development and testing of a general AMBER force field, J. Comput. Chem. 25 (2004) 1157–1174.
[42] M.W. Schmidt, K.K. Baldridge, J.A. Boatz, S.T. Elbert, M.S. Gordon, J.H. Jensen, S. Koseki, N. Matsunaga, K.A. Nguyen, S. Su, T.L. Windus, M. Dupuis, J.A. Montgomery Jr., General atomic and molecular electronic structure system, J. Comput. Chem. 14 (1993) 1347–1363.
[43] C.I. Bayly, P. Cieplak, W.D. Cornell, P.A. Kollman, A well-behaved electrostatic potential based method using charge restraints for determining atom-centered charges: the RESP model, J. Phys. Chem. 97 (1993) 10269–10280.
[44] D.A. Case, T.A. Darden, T.E. Cheatham III, C.L. Simmerling, J. Wang, R.E. Duke, R. Luo, R.C. Walker, W. Zhang, K.M. Merz, B. Roberts, S. Hayek, A. Roitberg, G. Seabra, J. Swails, A.W. Goetz, I. Kolossváry, K.F. Wong, F. Paesani, J. Vanicek, R.M. Wolf, J. Liu, X. Wu, S.R. Brozell, T. Steinbrecher, H. Gohlke, Q. Cai, X. Ye, J. Wang, M.-J. Hsieh, G. Cui, D.R. Roe, D.H. Mathews, M.G. Seetin, R. Salomon-Ferrer, C. Sagui, V. Babin, T. Luchko, S. Gusarov, A. Kovalenko, P.A. Kollman, AMBER 12, University of California, San Francisco, 2012.
[45] J.-P. Ryckaert, G. Ciccotti, H.J.C. Berendsen, Numerical integration of the Cartesian equations of motion of a system with constraints: molecular dynamics of n-alkanes, J. Comput. Phys. 23 (1977) 327–341.
[46] T. Mosmann, Rapid colorimetric assay for cellular growth and survival: application to proliferation and cytotoxicity assays, J. Immunol. Methods 65 (1983) 55–63.
[47] R.A. Laskowski, M.B. Swindells, LigPlot+: multiple ligand-protein interaction diagrams for drug discovery, J. Chem. Inf. Model. 51 (2011) 2778–2786.